NANO LETTERS
Letter
Cite This: Nano Lett. XXXX, XXX, XXX−XXX
pubs.acs.org/NanoLett

Dihydrolipoic Acid−Gold Nanoclusters Regulate Microglial Polarization and Have the Potential To Alter Neurogenesis

Lan Xiao,[†] Fei Wei,[†] Yinghong Zhou,[†,‡] Gregory J. Anderson,[§] David M. Frazer,[§] Yi Chieh Lim,[§] Tianqing Liu,*[,§] and Yin Xiao*[,†,‡]

[†]Institute of Health and Biomedical Innovation, Queensland University of Technology, 60 Musk Avenue, Kelvin Grove, Brisbane, QLD 4059, Australia

[‡]The Australia−China Centre for Tissue Engineering and Regenerative Medicine (ACCTERM), https://research.qut.edu.au/accterm/

[§]QIMR Berghofer Medical Research Institute, 300 Herston Road, Brisbane, QLD 4006, Australia

Supporting Information

ABSTRACT: Microglia-mediated neuroinflammation is one of the most significant features in a variety of central nervous system (CNS) disorders such as traumatic brain injury, stroke, and many neurodegenerative diseases. Microglia become polarized upon stimulation. The two extremes of the polarization are the neuron-destructive proinflammatory M1-like and the neuron-regenerative M2-like phenotypes. Thus, manipulating microglial polarization toward the M2 phenotype is a promising therapeutic approach for CNS repair and regeneration. It has been reported that nanoparticles are potential tools for regulating microglial polarization. Gold nanoclusters (AuNCs) could penetrate the blood−brain barrier and have neuroprotective effects, suggesting the possibility of utilizing AuNCs to regulate microglial polarization and improve neuronal regeneration in CNS. In the current study, AuNCs functionalized with dihydrolipoic acid (DHLA−AuNCs), an antioxidant with demonstrated neuroprotective roles, were prepared, and their effects on polarization of a microglial cell line (BV2) were examined. DHLA−AuNCs effectively suppressed proinflammatory processes in BV2 cells by inducing polarization toward the M2-like phenotype. This was associated with a decrease in reactive oxygen species and reduced NF-kB signaling and an improvement in cell survival coupled with enhanced autophagy and inhibited apoptosis. Conditioned medium from DHLA−AuNC-treated BV2 cells was able to enhance neurogenesis in both the neuronal cell line N2a and in an ex vivo brain slice stroke model. The direct treatment of brain slices with DHLA−AuNCs also ameliorated stroke-related tissue injury and reduced astrocyte activation (astrogliosis). This study suggests that by regulating neuroinflammation to improve neuronal regeneration, DHLA−AuNCs could be a potential therapeutic agent in CNS disorders.

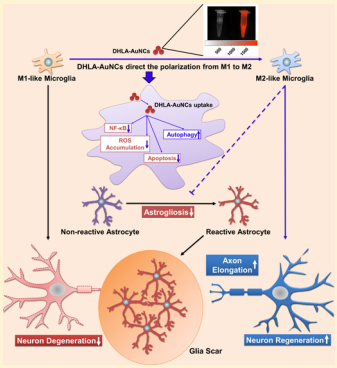

KEYWORDS: *Gold nanoclusters, neuroinflammation, microglial polarization, neuronal regeneration, immunomodulation*

Neuroinflammation, which contributes to neural damage and dysfunction, has been identified as a prominent pathological feature shared by central nervous system (CNS) disorders such as traumatic brain injury (TBI), stroke, and some neurodegenerative diseases including Parkinson's disease and Alzheimer's disease.[1−4] As the resident mononuclear phagocytes in the CNS parenchyma, microglia are an essential part of the CNS immune system and play an important role in tissue injury, repair, and regeneration.[4−8] When resting microglia are activated by external stimuli, such as pathogens or injury, they become polarized. The two extremes of this polarization are referred to as the M1-like and M2-like phenotypes.[8−12] M1 microglia are classically activated by proinflammatory cytokines such as interferon γ (IFNγ) or endotoxins such as lipopolysaccharide (LPS). When in this polarization state, microglia induce neuroinflammation by producing proinflammatory cytokines, nitric oxide (NO), and reactive oxygen species (ROS), which can lead to neural damage and impaired neurogenesis.[13,14] Moreover, M1 microglia can trigger astrocyte infiltration and activation (astrogliosis).[15] This can result in glial scar formation, which can form a barrier surrounding the injured region that prevents neuronal/axonal extension.[16,17] In contrast, M2 microglia are activated by interleukin 4 (IL-4) and IL-13, which induce neurogenesis and brain tissue regeneration by secreting anti-inflammatory neurotrophic factors such as IL-10, transforming growth factor-β (TGF-β), insulin-like growth factor 1 (IGF-1), basic fibroblast growth factor (bFGF), and brain-derived neurotrophic factor (BDNF).[4,14,18,19] The shift from M2 microglia to M1 microglia has been associated with increased injury progression in stroke and TBI.[20,21] Hence, modulating microglial polarization from M1 toward M2 is considered as a

Received: October 12, 2019
Published: November 30, 2019

DOI: 10.1021/acs.nanolett.9b04216
Nano Lett. XXXX, XXX, XXX−XXX

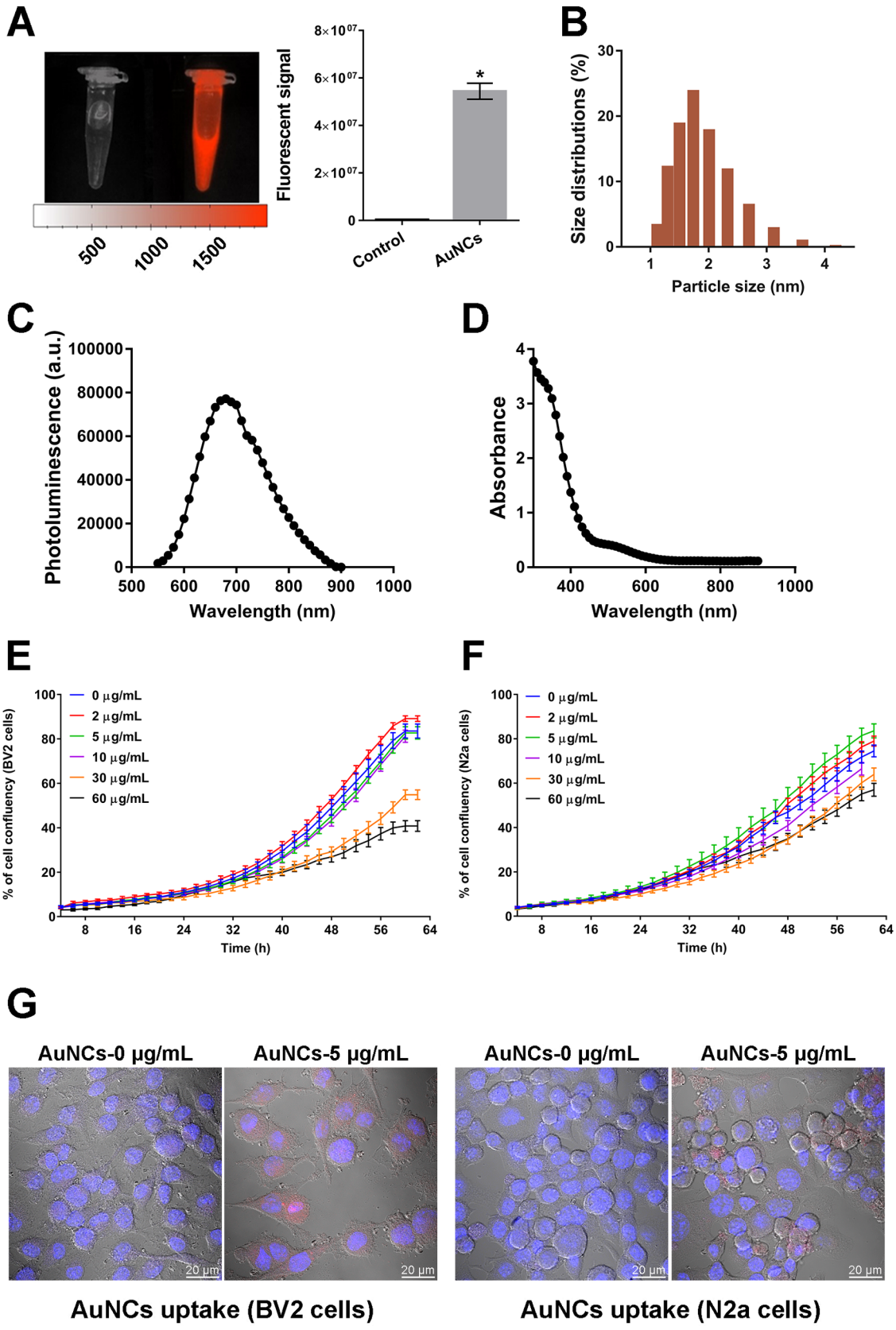

Figure 1. Characterization, biocompatibility, and cellular uptake of AuNCs. AuNCs were characterized by fluorescence intensity, size distribution, absorbance spectra, and fluorescence spectra (A–D). The time-dependent effects of AuNC application on the proliferation of BV2 and N2a cells were monitored by the IncuCyte ZOOM Live-Cell Analysis System. AuNC treatment resulted in reduced proliferation of BV2 (E) and N2a (F) cells with doses above 30 μg/mL (n = 9). (G) Intracellular AuNCs were observed in BV2 and N2a cells (treated with 0/5 μg/mL AuNCs) by confocal microscopy (AuNCs indicated by red signal, original magnification, 600×) with 405 nm excitation and a band-pass emission filter 685 nm/40 nm (center wavelength/width).

DOI: 10.1021/acs.nanolett.9b04216
Nano Lett. XXXX, XXX, XXX−XXX

potential therapeutic strategy for CNS regeneration and disease treatment.[8,13,22]

As oxidative damage and inflammation contribute to acute brain injury, antioxidant and anti-inflammatory drugs are in clinical use as neuroprotective agents for these disorders.[23] Lipoic acid, a natural lipophilic biomolecule with anti-inflammatory and antioxidant properties, can induce wound healing[24,25] and has demonstrated therapeutic benefits in heart and liver diseases, diabetes, and especially neurological disorders.[26−31] There are two forms of lipoic acid, known as α-lipoic acid (ALA, oxidized form) and dihydrolipoic acid (DHLA, reduced form).[32] ALA could be absorbed from the daily diet, transported to cells, and then reduced to DHLA.[33] Compared with ALA, DHLA has better antioxidant activity, which not only induces ROS scavenging but also facilitates the regeneration of endogenous antioxidants and the repair of oxidative damage.[34,35] Similar to ALA, DHLA has shown its capacities in anti-inflammation and neuronal protection,[36−39] suggesting its potential in regulating microglia-induced neuroinflammation.

Recent advances in nanotechnology suggest that nanoparticles are promising drug delivery systems for the treatment of CNS disorders.[40,41] Gold nanoclusters (AuNCs) are an emerging class of fluorescent nanomaterial that show potential as biomedical imaging and biosensing agents due to their unique size and optical properties, excellent photostability, and biocompatibility.[20,42−46] Furthermore, due to their ultrasmall size (<3 nm), AuNCs can also readily cross biological membranes and can penetrate the blood−brain barrier (BBB).[47] As AuNCs have been reported to stimulate immune response,[48] it is therefore necessary to examine whether this potential bioimaging tool would affect neuroinflammation or would the patient's health be impaired during diagnosis. AuNCs can be functionalized or protected with a range of chemical or biological molecules (such as DHLA[49,50]) by ligand exchange, bioconjugation, and noncovalent interaction, making them excellent candidates for brain targeted drug delivery.[51] It has been shown recently that *N*-isobutyryl-L-cysteine (L-NIBC) protected AuNCs have neuroprotective effects in an animal model of Parkinson's disease, although the mechanisms underlying the neuroprotection are not clear.[52] This raises the possibility of utilizing AuNCs for not only diagnosis but also treatment for CNS disorders by functionalizing them to regulate neuroinflammation. The neuroprotective and anti-inflammatory abilities of DHLA, combined with the brain penetrating capability of AuNCs, suggest that DHLA-functionalized AuNCs (DHLA−AuNCs) have therapeutic potential for neurological disorders; however, this has not been previously investigated.

In the current study, we hypothesized that DHLA−AuNCs could exert neuroprotective effects by regulating microglial polarization and thus improving neuronal regeneration. We investigated the effect of DHLA−AuNCs on polarization and proinflammatory responses in a microglial cell line (BV2 cells). We also examined the effect of this polarization on neuronal regeneration and astrogliosis using a neuronal cell line and an ex vivo stroke model (oxygen−glucose deprivation organotypic culture model). Our data suggest that DHLA−AuNCs restrained inflammation by directing BV2 cell polarization from M1 toward M2 under stimulated inflammatory conditions. Furthermore, conditioned medium generated by DHLA−AuNC-treated BV2 cells promoted neurogenesis at both the cellular and ex vivo tissue levels. In addition, DHLA−AuNC treatment ameliorated tissue damage in an ex vivo stroke model. Our results suggest that DHLA−AuNCs could be a potential neuroprotective agent for acute CNS injury.

RESULTS AND DISCUSSION

DHLA−AuNC Synthesis and Characterization. In this study, DHLA was used as a stabilizing agent for the preparation of AuNCs according to previously published protocols.[49] DHLA and $HAuCl_4$ were mixed with a small amount of the reducing agent $NaBH_4$. After microwave irradiation, the solution changed from a light yellow to a brownish color. DHLA−AuNCs showed intense red fluorescence (Figure 1A) under UV light in a Xenogen IVIS Imaging System. Dynamic light scattering (DLS) showed that the hydrodynamic diameter of the DHLA−AuNCs was 1.87 ± 0.14 nm (Figure 1B). The absorption spectrum exhibited a characteristic peak at approximately 700 nm (Figure 1C,D) as reported previously.[49] These results are consistent with a previous report of DHLA−AuNC synthesis.[49]

Previous studies have demonstrated that DHLA−AuNCs have good biocompatibility and show negligible toxicity to cells in culture.[49,53,54] In the current study, the proliferation profiles of BV2 (murine-microglia-derived cell line) and N2a (murine neuroblastoma cell line) cells cultured with DHLA−AuNCs at graded concentrations were examined by the IncuCyte ZOOM Live-Cell Analysis System. It could be observed that cells cultured with DHLA−AuNCs at high concentrations (above 30 μg/mL) showed decreased proliferation (Figure 1E,F). To determine whether the DHLA−AuNCs were overtly toxic, we examined whether they could affect the metabolism of BV2 or N2a cells using the 3-(4,5-dimethylthiazol-2-yl)-2,5-diphenyltetrazolium bromide (MTT) assay. After incubation with varying concentrations of DHLA−AuNCs, a dose-dependent reduction in the metabolic activity of both cell lines was observed (Figure S1A). However, no significant cytotoxicity was seen at concentrations $\leq$5 μg/mL. A time-dependent cell metabolism change was examined by alamarBlue cell viability assay on BV2 and N2a cells. Similarly, DHLA−AuNCs at concentrations $\leq$10 μg/mL did not affect the metabolism of BV2 cells within 24 h, while for 48 and 72 h, a dose-dependent metabolism decrease could be found on BV2 cells treated with DHLA−AuNCs at concentrations higher than 5 μg/mL (Figure S1B). For N2a cells, DHLA−AuNCs at concentrations higher than 30 μg/mL were found to downregulate cell metabolism on 72 h of culture (Figure S1B). Cell survival rate was determined after 72 h of culture via trypan blue staining, and the percentage of live cells was calculated by the Countess II Automated Cell Counter. A nonsignificant difference on viability could be found in cells treated with AuNCs at concentrations below 5 μg/mL (Figure S1C). Taking consideration of all these results, concentrations of DHLA−AuNCs up to 5 μg/mL were used in subsequent studies. Our data suggest that cell toxicity is unlikely to be a concern in potential therapeutic applications of DHLA−AuNCs as long as concentrations of the nanoparticles are kept below 5 μg/mL.

Previous studies have shown that DHLA−AuNCs (hereafter simply referred to as AuNCs) can be effectively taken up by HeLa cells.[49,53,54] Due to their inherent fluorescent properties, the internalized AuNCs can be visualized, and their fluorescent signal remains stable for at least 2 h.[49,53,54] We demonstrated that AuNCs behaved similarly in BV2 and N2a cells and observed intracellular AuNCs for up to 24 and 48 h in BV2 and N2a cells, respectively (Figures 1G and S1D). MTT assays

DOI: 10.1021/acs.nanolett.9b04216
Nano Lett. XXXX, XXX, XXX−XXX

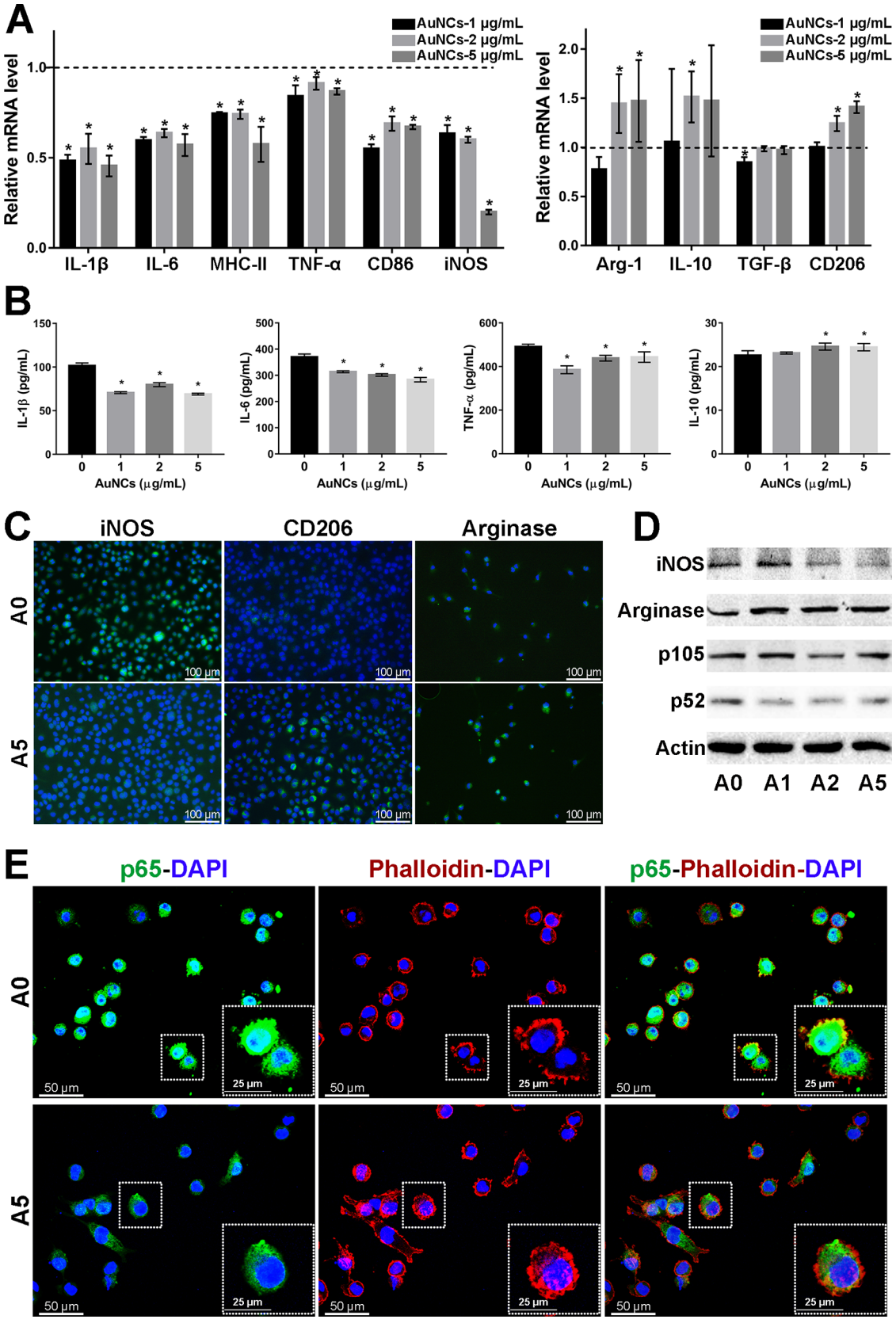

Figure 2. Effect of AuNCs on the proinflammatory response of BV2 cells, which were treated with AuNCs (0/1/2/5 μg/mL, AuNCs-0 μg/mL served as the control group) during inflammatory stimulation (LPS + IFNγ) for 24 h. (A) The represented mRNA levels of AuNCs-1/2/5 μg/mL groups were normalized to the control group and appeared as fold changes. In cells treated with AuNCs, mRNA levels of proinflammatory M1-like markers (*IL-1β*, *IL-6*, *MHC-II*, *TNF-α*, *CD86*, *iNOS*) were significantly downregulated, whereas the levels of anti-inflammatory M2-like markers (*Arg-1*, *IL-10*, *CD206*) were significantly upregulated, when compared to the controls. The dotted lines indicated the relative expression levels (fold = 1) in the control group. Data are presented as the mean ± SD ($n = 3$). *$P < 0.05$ versus the control group. (B) Quantification of cytokines in BV2

DOI: 10.1021/acs.nanolett.9b04216
Nano Lett. XXXX, XXX, XXX−XXX

Figure 2. continued

cell supernatant was performed by ELISA. AuNC treatment resulted in decreased secretion of inflammatory cytokines (IL-1β, IL-6, TNF-α) while increasing the production of the anti-inflammatory cytokine IL-10 after 24 h of stimulation. Data are presented as the mean ± SD (n = 3). *P < 0.05 versus the control group. (C) Represented IF staining images of iNOS, CD206, and arginase (Alexa Fluor488, green) in BV2 cells. Nuclei were counterstained with DAPI (blue). BV2 cells treated with AuNC-5 μg/mL showed reduced expression of iNOS (M1-like) and induced expression of CD206 and arginase (M2-like), as compared with the A0 control group (original magnification, 200×). (D) Protein levels were examined by Western blotting analysis. Results showed that the protein levels of iNOS and NF-κB p52 were downregulated following AuNC application, while arginase expression was induced in AuNC-treated cells. (E) IF staining of NF-κB p65 (Alexa Fluor488, green) showed that in comparison with the control group, the cytoskeleton−nuclear translocation of p65 (original magnification, 400×) was reduced in cells treated with AuNCs (5 μg/mL). Cell cytoskeleton was stained with phalloidin (BODIPY 558/568, red). Nuclei were stained with DAPI (blue). A0/1/2/5 = BV2 cells applied with AuNCs-0/1/2/5 μg/mL.

showed that the AuNCs had a minimal impact on cellular metabolism over this period, so similar timeframes were used in subsequent in vitro studies.

AuNC Treatment Suppresses Proinflammatory Responses in a Microglial Cell Line by Inducing Polarization toward the M2 Phenotype. To investigate the effect of AuNCs on BV2 polarization, these cells were stimulated with LPS and IFNγ to mimic the inflammatory environment as previously described.[55−57] Cells treated with up to 5 μg/mL AuNCs were tested (AuNCs-0 μg/mL served as the control group). As shown in Figures S2A and 2A, after 12 or 24 h treatment, AuNCs significantly downregulated the mRNA levels of the M1-like markers[58,59] *MHC-II*, *CD86*, and *iNOS*, while those for the M2-like markers[58,59] *Arg-1* and *CD206* were significantly elevated. The mRNA levels of various pro/anti-inflammatory cytokines (*IL-1β*, *IL-6*, *TNF-α*/*IL-10*) were found to be reduced/induced following AuNC treatment for 24 h (Figure 2A), and these results were validated by measuring the production of cytokines in the supernatant (Figure 2B). Likewise, AuNCs reduced the level of iNOS protein, an intracellular marker of the M1-like phenotype (Figures 2C,D and S2C,D). We also observed a dose-dependent increase in the production of the M2-like protein markers CD206 (Figures 2C and S2C) and arginase (Figures 2C,D and S2C,D) following AuNC treatment. Collectively, these data imply that AuNCs induce the conversion of the microglia-derived BV2 cells from a M1-like phenotype to a M2-like phenotype, thereby suppressing proinflammatory responses. A comparison was also made between DHLA and AuNCs at the same molar concentration of DHLA (Figure S3). As expected, DHLA alone also inhibited the inflammatory phenotype when compared with the control group; however, the magnitude of the effects was less than that seen with AuNCs. Especially, a significantly induced protein level of iNOS (M1) was found in DHLA-treated cells, which also showed reduced expression of M2-like marker arginase (Figure S3C), suggesting the DHLA-directed inflammation suppression is not as effective as the one directed by AuNCs.

M1 microglia act as suppressors of neurogenesis and are thought to contribute to many neurodegenerative diseases.[1,2] The detrimental roles of M1 microglia are due to the release of inflammatory cytokines.[1,2] Microglia-derived IL-1β and TNF-α act as neurotoxins and can cause neural damage and retard neurogenesis.[60−62] They can also disrupt the BBB, allowing the infiltration of immune cells and triggering the inflammatory cascade.[60−62] IL-6 is another inflammatory cytokine produced by M1 microglia and has been demonstrated to suppress neurogenesis while facilitating astrogliosis.[63] In addition to the production of inflammatory cytokines, the upregulation of iNOS in M1 microglia leads to the overproduction of nitric oxide (NO), which can result in neural apoptosis or necrosis via stimulation of *N*-methyl-D-aspartate (NMDA) receptors.[64−66] In contrast, M2 microglia enhance neural tissue regeneration by producing beneficial neurotrophins and anti-inflammatory cytokines.[22] For example, IL-10 has been shown to induce neurogenesis and the migration of neural progenitor cells, facilitating neural repair.[67] In the current study, we found that AuNC treatment of a microglia-derived cell line reduced the expression of M1-like markers while inducing that of M2-like markers at both the mRNA and protein levels. These data raise the possibility that AuNCs could exert a neuroprotective effect in vivo.

AuNCs Downregulate the NF-κB Signaling Pathway in BV2 Cells Following an Inflammatory Stimulus. Further investigations were carried out to examine the mechanism(s) by which AuNCs affected BV2 cells. The nuclear factor kappa-light-chain-enhancer of activated B cells (NF-κB) signaling pathway is essential for the macrophage/microglial inflammatory response, including proinflammatory cytokine secretion and iNOS expression/NO release.[68−71] The activation of the NF-κB signaling pathway is characterized by the translocation of the p65 subunit from the cytoplasm to the nucleus and by an increase in the expression of the p52 subunit.[72,73] Immunofluorescent (IF) staining showed that AuNCs inhibited nuclear translocation of NF-κB p65 in BV2 cells (Figures 2E and S4); in addition, Western blotting showed a significant decrease in p52 protein levels (Figures 2D and S2D) when compared to the control group. These results suggest that the inhibition of the NF-κB signaling pathway likely contributes to the AuNC-induced suppression of the proinflammatory response in BV2 cells.

AuNCs Can Scavenge ROS during the Proinflammatory Response in BV2 Cells. Previous studies have demonstrated a fundamental role for ROS in the microglial proinflammatory response.[13,74] ROS are also involved in brain cell apoptosis and can contribute to postinjury neuronal loss in CNS pathologies such as stroke and TBI.[75−78] Inflammatory stimuli, such as TNF-α and LPS, can induce cellular ROS production in microglia through the activation of nicotinamide adenine dinucleotide phosphate oxidase (NOX) and mitochondria.[75,79] Once produced, ROS interact with the NF-κB signaling pathway to activate the inflammasome and stimulate proinflammatory cytokine secretion.[79−81] In the current study, ROS production by BV2 cells was detected by flow cytometry analysis following 2′,7′-dichlorodihydrofluorescein diacetate (H_2DCFDA) staining as previously described.[82−84] As shown in Figure 3A, an inflammatory stimulus resulted in ROS accumulation in BV2 cells (86.5% of cells in the control group were ROS-positive), which is in accordance with the previous studies.[13,74,85] ROS production was inhibited in a dose-

DOI: 10.1021/acs.nanolett.9b04216
Nano Lett. XXXX, XXX, XXX−XXX

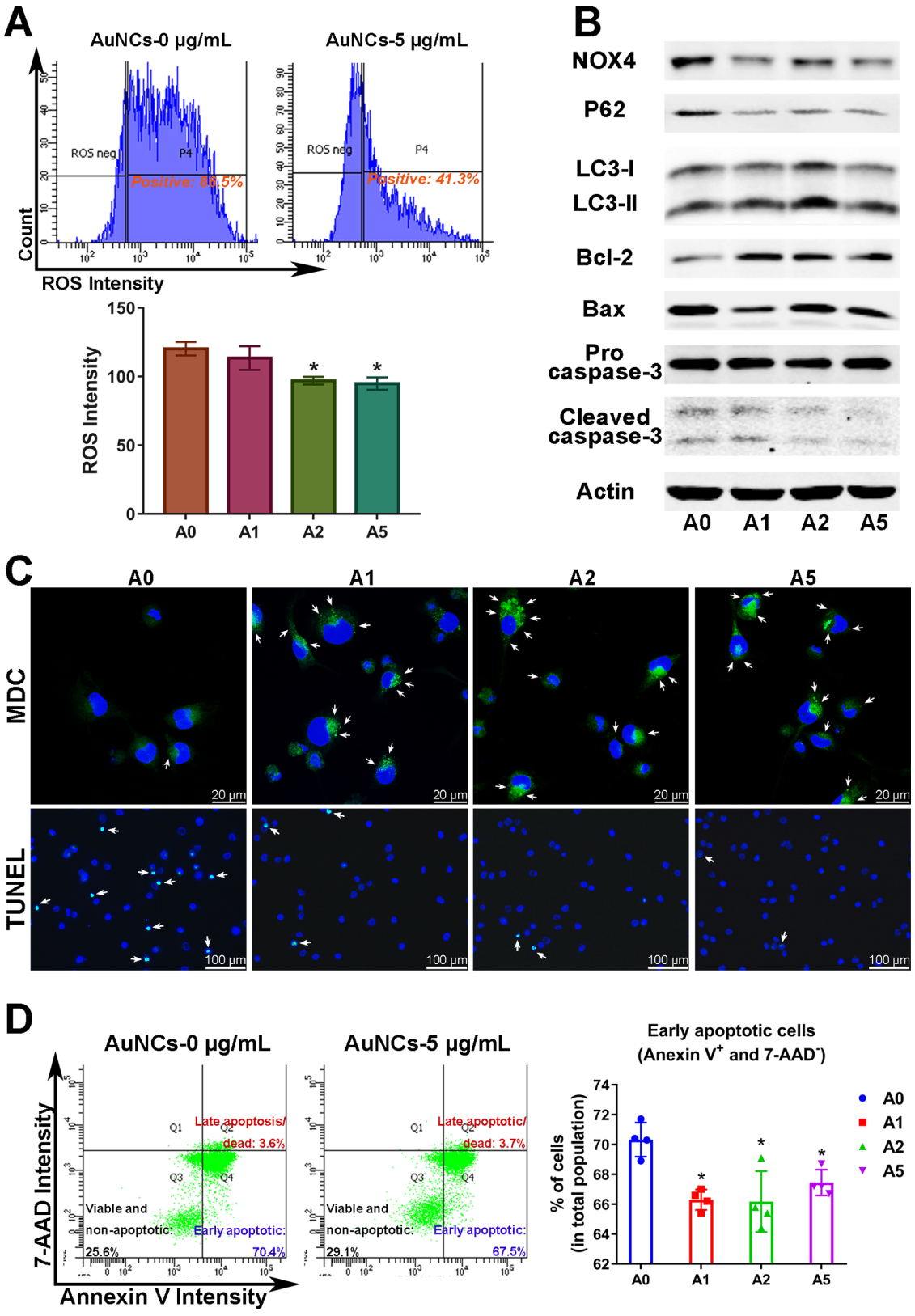

Figure 3. AuNC application resulted in induced autophagy and reduced ROS and apoptosis in BV2 cells with an inflammatory stimulus (LPS + IFNγ) for 24 h. (A) ROS production was measured by flow cytometry analysis of H2DCFDA stained BV2 cells. The result showed that AuNCs (5 μg/mL) downregulated the percentage (41.3%) of ROS-positive cells, as compared with the A0 control group (86.5%). Quantification of ROS intensity showed that AuNCs reduced ROS in BV2 cells in a dose-dependent manner. Data are presented as the mean ± SD (n = 3). *P < 0.05 versus the control group. (B) Protein levels in BV2 cells were examined by Western blotting analysis regarding NOX4 (ROS/oxidative stress-related); p62, LC3 (autophagy-related); Bcl-2, Bax, caspase-3 (apoptosis-related), respectively. (C) Autophagy was detected in BV2 cells via MDC staining. AuNC application led to induced autophagosome formation (MDC-positive green sphere-like structures, as indicated by arrows) in BV2 cells (original magnification, 600×). Apoptosis was detected in BV2 cells with TUNEL staining. The TUNEL signal (green nuclei indicated by

DOI: 10.1021/acs.nanolett.9b04216
Nano Lett. XXXX, XXX, XXX−XXX

Figure 3. continued

arrows, original magnification, 200×) was reduced in AuNC-treated cells. (D) Annexin V/7-AAD flow cytometry assay of BV2 cells upon inflammatory stimulation. Cells were separated into early apoptotic (annexin V^+/7-AAD^-), viable and nonapoptotic (annexin V^-/7-AAD^-), and late apoptotic/dead (annexin V^+/7-AAD^+) cells. AuNC-treated BV2 cells showed significantly reduced apoptosis (percentage of annexin V^+/7-AAD^- cells in total population, $^*P < 0.05$ versus the A0 control group). Data are presented as the mean ± SD ($n = 4$). A0/1/2/5 = BV2 cells with AuNCs at 0/1/2/5 μg/mL.

dependent manner in AuNC-treated BV2 cells relative to controls, as shown by reduced percentages of ROS-positive cells (86.5% at control vs 41.3% at 5 μg/mL AuNCs; $P < 0.05$, Figures 3A and S5A) and downregulated ROS intensity (Figure 3A). Consistently, the level of NOX4 protein (a member of the NOX family, a marker for ROS/oxidative stress[86−88]) was significantly decreased in BV2 cells treated with AuNCs (Figures 3B and S5B). However, this decrease was not in a dose-dependent manner, suggesting that other members of the NOX family, e.g., NOX1/3 or DUOX1/2, might also be involved in the downregulation of ROS.[89] Alternatively, the restricted ROS accumulation might be due to the clearance of mitochondria by cellular processes such as autophagy.[90−92] These data indicate that the AuNC-mediated reduction of the BV2 inflammatory response is at least partially due to a decrease in ROS production.

AuNCs Induce Autophagy and Reduce Apoptosis in BV2 Cells. Further investigation was performed to find the possible reason for the decreased ROS production. The apoptosis-mediated microglial cell death is found in many CNS disorders and is associated with neuroinflammation, although the mechanisms are not well-defined.[93] This reduces the number of microglia available for neural repair, thereby facilitating disease progression and leading to a worse prognosis for the patient.[13,93−95] In contrast, autophagy, which describes the breakdown and recycling of cellular components,[96,97] can reduce apoptosis and promote cell survival by removing damaged mitochondria, thereby preventing the release of proapoptotic proteins and other factors into the cytosol.[90−92] This process is partially achieved via p62 (also known as sequestosome-1/SQSTM1), which selectively binds with damaged mitochondria and LC3 to facilitate degradation by autolysosome.[92,98,99] Furthermore, this elimination of damaged mitochondria reduces ROS accumulation, which in turn suppresses inflammation by interrupting the activation of inflammasome (Scheme 1).[98,100−102] This suggests that the regulation on autophagy/apoptosis balance should facilitate ROS clearance and thereby downregulate inflammatory response. Of note, autophagy is also related with cell death, a phenomenon termed as "autophagic cell death (ACD)" characterized by the appearance of large-scale autophagic vacuolization in cell cytoplasm accompanied by the absence of chromatin condensation.[103] However, it is still controversial whether ACD is cell death because of autophagy or cell death with autophagy.[103] A recent study has found a special autophagy gene-dependent cell death termed as "autosis", which is mediated by the Na^+, K^+−ATPase pump.[104] It is speculated that although autophagy is a strategy to maintain homeostasis and induce survival for cell under stress conditions, excessive or uncontrolled levels of autophagy may result in ACD,[105] suggesting the autophagy level should be maintained at certain levels to achieve its beneficial effects.

We then sought to evaluate the autophagy/apoptosis balance in AuNC-treated BV2 cells. To examine autophagy in AuNC-treated BV2 cells following an inflammatory stimulus, the presence of autophagosomes (vesicles containing cellular components to be degraded) was determined using the fluorescent dye dansylcadaverine (MDC).[106−110] MDC-positive puncta (green sphere-like structures, as indicated by arrows in Figure 3C) increased in AuNC-treated cells when compared to controls, implying that AuNCs induce autophagosome formation in BV2 cells. We also observed a partial colocalization of autophagosomes with AuNCs in the cytosol (Figure S5C), suggesting a possible interaction between AuNCs and autophagocytic vesicles. A prominent marker of autophagy is the conjugation of the cytosolic form of microtubule-associated protein 1A/1B-light chain 3 (LC3-I) with phosphatidylethanolamine to form LC3-II, which then associates with the autophagosomal membrane.[109,111−114] Consistent with autophagy, Western blotting showed an increase in the ratio of LC3-II to LC3-I in AuNC-treated BV2 cells (Figures 3B and S5B). Furthermore, p62, which is degraded during autophagy,[109,115] was reduced after AuNC treatment (Figures 3B and S5B). These data demonstrate that AuNC treatment induces autophagy in BV2 cells following an inflammatory stimulus.

We then examined the effect of AuNCs on apoptosis in BV2 cells previously subjected to an inflammatory stimulus. Terminal deoxynucleotidyl transferase dUTP nick end labeling (TUNEL)[116] showed a reduced signal in AuNC-treated cells compared with control cells (Figure 3C). Apoptosis was also examined using flow cytometry and the annexin V/7-AAD assay as previously described,[117−120] and the whole cell population of each group was divided into four squares consisting of annexin V^-/7-AAD^- cells (viable and nonapoptotic), annexin V^+/7-AAD^- cells (early apoptotic), annexin V^+/7-AAD^+ cells (late apoptotic/dead cells), and annexin V^-/7-AAD^+ cells (Figures 3D and S6A). Treatment with AuNCs resulted in a decrease in the percentage of early apoptotic cells (annexin V^+/7-AAD^- decreased from 70.4% in the control group to 67.5% in the AuNCs-5 μg/mL group, $P = 0.022$) while increasing the percentage of viable and nonapoptotic cells (annexin V^-/7-AAD^- increased, from 25.6% in the control group to 29.1% in the AuNCs-5 μg/mL group, $P = 0.013$) (Figures 3D and S6A,B). There was no significant difference on the percentage of late apoptotic/dead cells (annexin V^+/7-AAD^+, Figure S6B). To avoid the possible annexin V increasement resulted from cell detachment,[121] a direct annexin V/PI staining was performed on BV2 cells seeded on a 96-well plate, and the results showed much lower annexin V intensity in AuNC-treated BV2 cells (Figure S6C). No significant difference could be found in PI intensity (Figure S6C), suggesting there is no difference in cell viability at this time point of stimulation (24 h). Consistently, the conversion of pro-caspase-3 to cleaved caspase-3, another apoptosis marker,[122] was reduced in a dose-dependent manner in AuNC-treated BV2 cells (Figures 3B and S5B). AuNCs also significantly induced the expression of Bcl-2 (antiapoptotic) while reducing the expression of Bax (proapoptotic) (Figures 3B and S5B).[123,124] In addition, we monitored BV2 cell

DOI: 10.1021/acs.nanolett.9b04216
Nano Lett. XXXX, XXX, XXX−XXX

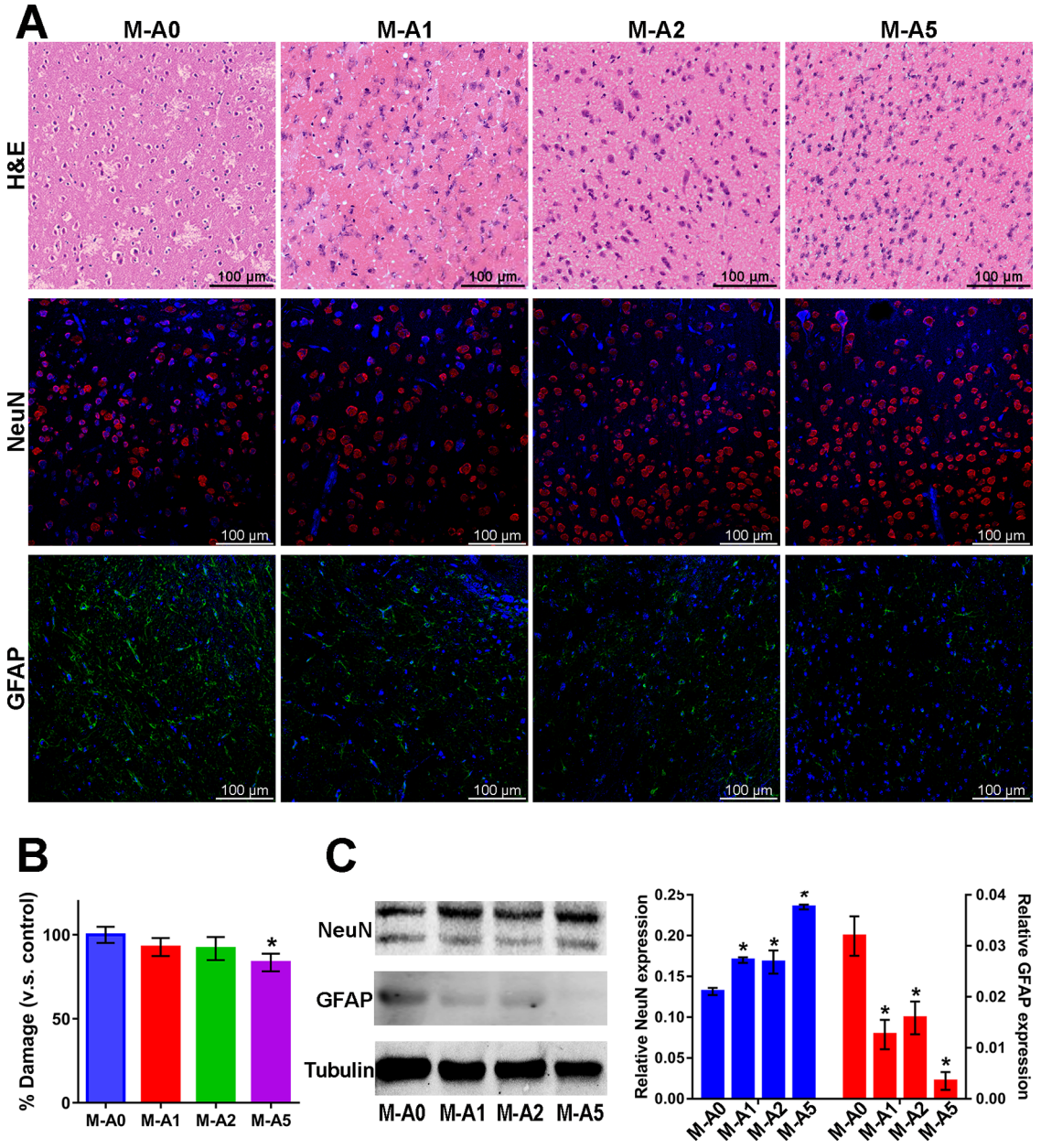

Figure 4. AuNC-treated BV2 cell-originated CM improved neurogenesis and restrained astrogliosis in an ex vivo OGD brain slice model. (A) The OGD-stimulated mouse brain slice model was applied with CM originated from AuNC-treated BV2 cells. H&E staining was performed for histological observation, as shown in the represented images (original magnification, 200×). The IF staining results showed that AuNC-treated BV2 cell-derived CM (Group M-A1/2/5) induced NeuN (Alexa Fluor 568, red) expression and reduced that of GFAP (Alexa Fluor 488, green) in OGD brain tissue (original magnification, 200×). (B) PI staining and quantification was performed to detect cell death in live OGD brain tissue, which was normalized against the M-A0 group. Results showed significantly reduced PI-positive cells in brain tissue applied with CM from BV2 cells treated by 5 μg/mL AuNCs (Group M-A5). (C) Protein levels of NeuN and GFAP were examined by Western blotting analysis in OGD brain tissue. CM from AuNC-treated BV2 cells resulted in induced/reduced protein levels of NeuN/GFAP, respectively. M-A0 = OGD brain tissues treated with CM from the control BV2 cells. M-A1/2/5 = OGD brain tissues treated with CM from BV2 cells applied with AuNCs-1/2/5 μg/mL. All data are presented as the mean ± SD (n = 3). *P < 0.05 versus M-A0 control group.

viability using a real-time live cell imaging and found that the continuous inflammatory stimulus resulted in a drastic decrease in cell viability after 40 h of stimulation (as compared with the blank control—Group Normal in Figure S6D). However, the treatment of AuNCs was able to overcome this effect and increase cell survival in a dose-dependent manner (Figure S6D) at those late time points (post-40 h). Taken together, these data suggest that AuNCs decrease the frequency of apoptosis in BV2 cells during inflammation, and this may be mediated through the induction of autophagy.

Previous studies have found that nanoparticles can activate or inhibit autophagy depending on their physicochemical properties, leading to either cell survival or cell death, although the mechanisms involved are poorly understood.[125,126] In the current study, we found that AuNCs induce cell autophagy while reducing apoptosis and cell death in BV2 cells. It is also reported that nanoengineered surface modulation (allylamine-

DOI: 10.1021/acs.nanolett.9b04216
Nano Lett. XXXX, XXX, XXX−XXX

coated surface seeded with gold nanoparticles) regulates macrophage immune responses by inducing autophagy, suggesting autophagy could be a potential target for immunomodulation in regenerative medicine.[127] Based on the current results, we predict that AuNCs regulate the autophagy−apoptosis balance by promoting autophagy, which, at least in part, interrupts the inflammatory cascade by scavenging ROS and reducing NF-kB signaling (Scheme 1 in the Supporting Information). This AuNC-directed regulation on the autophagy/apoptosis balance might be the reason for the increased viability at the very late stage (40 to 72 h, Figure S6D) of inflammatory stimulation, but this requires further investigation. The effects of DHLA on autophagy/apoptosis were also examined in DHLA-treated BV2 cells. Interestingly, compared to AuNC-treated cells, DHLA (at high concentration) treatment increased both autophagy and apoptosis levels (increased LC3-II to LC3-I ratio, increased the cleaved caspase-3 to pro-caspase-3 ratio, Figure S6E) in BV2 cells under inflammatory stimulus, suggesting the mechanisms under DHLA- and AuNC-directed immunomodulation might be different, which still needs further investigation in the future. It should be noted that in AuNCs, DHLA acts like "glue" between Au atoms to bind them together to form AuNCs, which raises a question of whether DHLA at this form would still act in a similar way to the free DHLA. Further investigation is required to verify this point in the future.

Factors Secreted by AuNC-Treated BV2 Cells Improve Neurogenesis in Vitro and ex Vivo. To investigate whether BV2 cells treated with AuNCs could release factors that may contribute to neuronal regeneration, N2a cells were treated with BV2 conditioned medium (CM) during retinoic-acid-induced neuronal differentiation.[128,129] Expression of NeuN, a neuronal nuclear antigen and differentiation marker,[130] was examined using IF as previously described.[131,132] There was much stronger NeuN staining in N2a cells treated with CM obtained from AuNC-treated BV2 cells (Groups M-A1 to M-A5) compared to those treated with CM from control cells (Group M-A0) (Figure S7A). This increase in NeuN expression was confirmed by Western blotting (Figure S7B). An earlier stage neuronal marker, nestin, was also examined,[133] and the result showed that nestin expression was significantly induced in N2a cells with CM from AuNC-treated BV2 cells (Figure S7B). Enhanced axonal elongation and neurite outgrowth were also observed in differentiating N2a cells treated with CM from AuNC-treated BV2 cells (Figure S7A). Quantitative analysis showed significantly increased average neurite length (Figure S7C) when N2a cells were incubated with CM from AuNC-treated BV2 cells. Changes in cellular morphology, as measured by cell eccentricity, showed similar trends, with CM from AuNC-treated BV2 cells significantly increasing cell eccentricity after 12.5 h (Figure S7D). This suggests that AuNCs induce BV2 cells to secret factors relatively beneficial for axonal elongation and thus neuronal differentiation.

To compare the effects of DHLA- and AuNC-directed immunomodulation on neuronal regeneration, CM derived from DHLA-treated BV2 cells was also investigated on N2a cells during differentiation, and the effects were compared with those of CM from AuNC-treated BV2 cells. As shown in Figure S8, both the CM from DHLA- and AuNC-treated BV2 cells led to increased axonal elongation and neurite outgrowth in N2a cells (Figure S8A) as well as an induced protein level of nestin (Figure S8B), as compared with the M-A0 group. CM from AuNC-treated BV2 cells showed enhanced neurite length and induced expression of later neuronal marker NeuN, while the earlier neuronal marker nestin expression was reduced, as compared with those treated with CM from DHLA-treated BV2 cells (Figure S8A,B). These results suggest that CM from AuNC-treated BV2 cells could improve neuronal differentiation toward a more mature stage. Therefore, these results further demonstrate that AuNCs are more effective than DHLA on immunomodulation and neuronal regeneration.

The beneficial effects of CM from BV2 cells treated with AuNCs were further examined in an ex vivo stroke model. The organotypic brain slice culture system is a well-established ex vivo model that is widely used for neurological research.[134,135] This brain slice model preserves the original brain tissue architecture and neuronal activities and maintains functional local synaptic circuitry, while increasing experimental accessibility and allowing the precise manipulation of the extracellular microenvironment.[134,135] In the current study, an oxygen/glucose deprivation (OGD)-induced mouse brain slice stroke model[135−137] was used to study the effect of CM from AuNC-treated BV2 cells on neuroinflammation-related neuronal degeneration and astrogliosis. Cell death in live brain slices was evaluated with propidium iodide (PI) staining, as this dye cannot cross the plasma membrane of live cells.[138] CM from BV2 cells treated with 5 μg/mL AuNCs significantly reduced the number of PI-positive cells under OGD conditions (Group M-A5, $P = 0.018$), although no effect was seen with CM from BV2 cells treated with lower concentrations of AuNCs (Groups M-A1−2, Figure 4B). Inflammatory cytokines from BV2 cells (e.g., IL-1β)[60−62] could be responsible for exacerbating OGD-mediated cell death. Although AuNCs at low doses (1−2 μg/mL) suppressed the proinflammatory response in BV2 cells (Figure 2), the effect was not as obvious as in those treated with a high dose of AuNCs (5 μg/mL). Thus, the soluble mediators in the CM from BV2 cells treated with low doses of AuNCs likely did not reach a sufficient threshold to ameliorate cell death in the OGD model.

Pathological changes in the brain tissue were also assessed using hematoxylin and eosin (H&E) staining. As seen in Figure S9, compared with the normal brain tissue, OGD resulted in neuron loss, cytoplasm vacuolation, and shrinkage in the cerebral cortex, which are typical pathological changes seen in stroke affected brain tissue.[139] The OGD brain tissue treated with CM from control cells (Group M-A0, Figures 4A and S9) showed similar pathological changes, while CM from AuNC-treated BV2 cells (Groups M-A1−5) reduced these changes (reduced cell vacuolation and shrinkage). These results suggest that CM from AuNC-treated cells alleviates tissue damage in the OGD stroke model.

We also found NeuN increased, and glial fibrillary acidic protein (GFAP) decreased (Figure 4A,C) in brain slices treated with CM from AuNC-treated BV2 cells. GFAP is an intermediate filament protein expressed by activated astrocytes.[15,16,140] Astrocytes can be activated by M1 microglia.[141] Activated astrocytes lose the normal astrocyte functions beneficial for neurogenesis (e.g., promoting neuronal survival and outgrowth, inducing synaptogenesis and phagocytosis) while producing neurotoxic factors that can induce the rapid death of neurons and mature oligodendrocytes and can contribute to postinjury neuron degeneration.[141] They are also the main cellular component of glial scars, which hinder neural repair by blocking the axonal elongation and connection.[16,17] Our results suggest that AuNCs potentially

DOI: 10.1021/acs.nanolett.9b04216
Nano Lett. XXXX, XXX, XXX−XXX

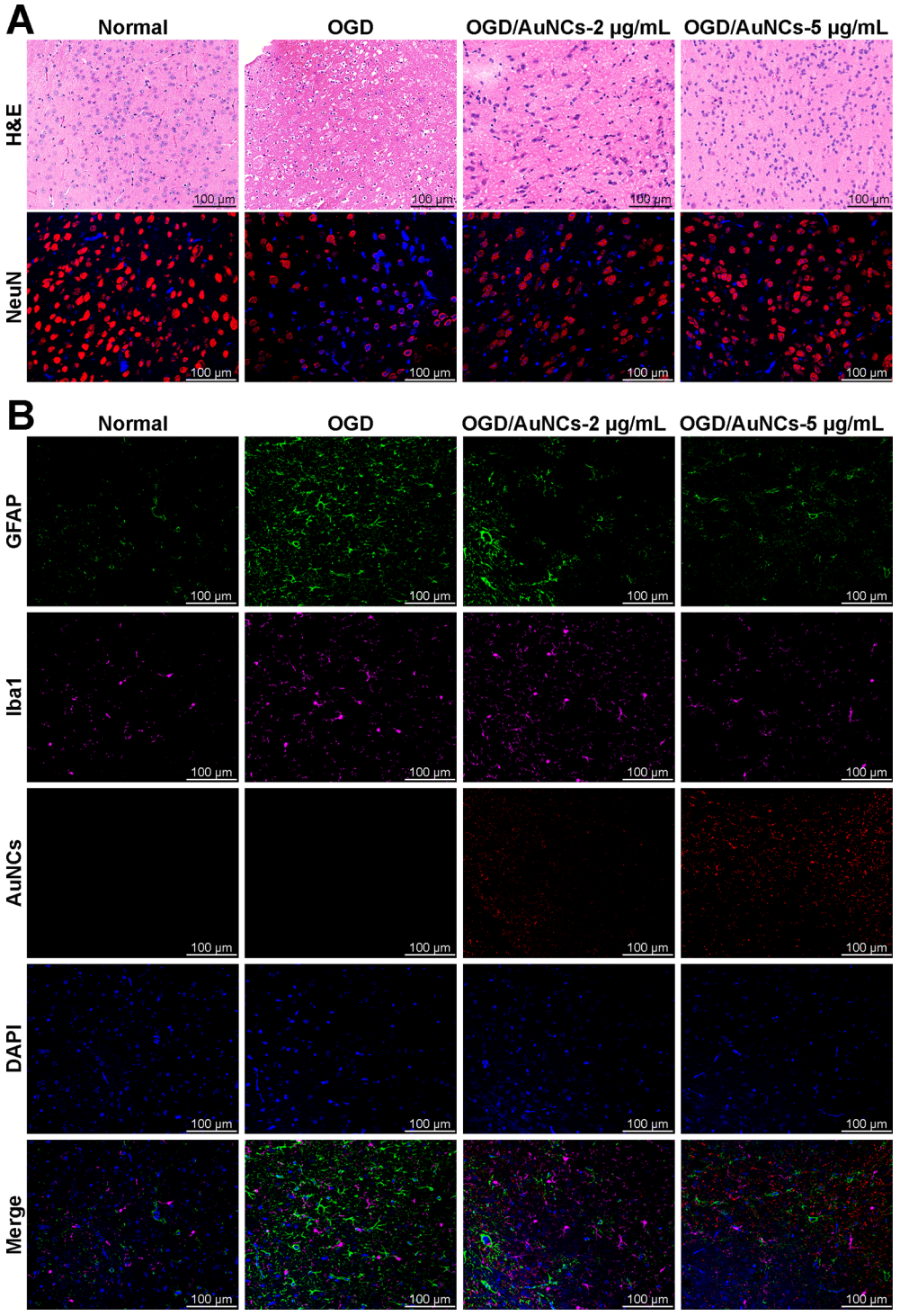

Figure 5. Therapeutic effect of AuNCs in ex vivo OGD model. OGD brain slice model was applied with AuNCs (2/5 μg/mL), and the effect was evaluated by histological observation and IF staining. (A) H&E staining images indicated the histological abnormities of OGD brain tissues, which were alleviated following AuNC treatment. Compared with the normal control, NeuN (Alexa Fluor 568, red) expression was impaired in OGD brain, which was then restored by AuNCs (original magnification, 200×). (B) The distribution of reactive astrocytes (GFAP, Alexa Fluor 488, green), microglia (Iba-1, Alexa Fluor 647, purple), and AuNCs (red) was colocalized in normal/OGD brains. The expression of GFAP/Iba-1 was induced in OGD brain as compared with that in the normal control, which was then downregulated following AuNCs application (original magnification, 200×). Nuclei were stained with DAPI (blue). Normal = untreated healthy brain tissue. OGD = brain tissue with OGD stimulation. OGD/AuNCs-2/5 μg/mL = OGD-stimulated brain tissue with AuNC application (2/5 μg/mL).

could induce M1-like microglia to produce less inflammatory and more tissue-regenerative factors, which, in turn, increases neurogenesis and inhibits astrogliosis, but this will need to be further verified in vivo in the future.

AuNCs Directly Induce the Differentiation of N2a Cells in Vitro. To investigate whether AuNCs had direct effects on neurogenesis, N2a cells were treated with AuNCs during induced neuronal differentiation. AuNCs enhanced

DOI: 10.1021/acs.nanolett.9b04216
Nano Lett. XXXX, XXX, XXX−XXX

NeuN protein expression during neurogenesis, as determined by IF (Figure S10A) and Western blotting (Figure S10B). The nestin expression was also increased in AuNC-treated cells (Figure S10B). N2a cells treated with AuNCs also showed greater axonal elongation and enhanced neurite outgrowth (Figure S10A,C). This effect was dose-dependent and was consistent with the increase in eccentricity observed after treating N2a cells with AuNCs for 12.5 h (Figure S10D). These data suggest a direct beneficial effect of AuNCs on neuronal regeneration.

To determine the effect of DHLA alone on neurogenesis, N2a cells were treated with AuNCs or an equimolar dose of DHLA and neuronal morphology and nestin/NeuN expression was examined. Both AuNCs and DHLA induced axonal elongation and neurite outgrowth (Figure S11A) and nestin/NeuN expression (Figure S11C,D) in differentiating N2a cells. However, AuNC-treated cells showed significantly longer average neurite lengths (Figure S11A) and greater cell eccentricity (Figure S11B) than those treated with DHLA, although there was no significant difference between the AuNC-treated and DHLA-treated groups (at high concentrations) with respect to nestin/NeuN expression at low or high concentrations (Figure S11C,D). Overall, these data suggest that AuNCs and DHLA show similar neurorestorative properties in vitro.

Treatment with AuNCs Ameliorates Neuroinflammation and Astrogliosis while Facilitating Neurogenesis in an ex Vivo Stroke Model. We also investigated whether AuNCs could exert a direct neuroprotective effect in our ex vivo brain slice model under OGD conditions. Damaged cerebral cortex tissue was observed in the OGD stroke model, while tissue integrity was maintained in the untreated control (Figure 5A). AuNC treatment led to a significant reduction in the severity of OGD-induced tissue injury, and this was associated with decreased cell shrinkage and reduced vacuolation (Figure 5A). We then studied the three main cell populations in the cortex using IF staining against NeuN (neuronal marker), GFAP (astrocyte marker), and ionized calcium binding adaptor molecule 1 (Iba-1, microglial marker).[142] In comparison to the normal control, there were far fewer NeuN-positive cells in the OGD group, whereas treatment with AuNCs ameliorated this decrease (Figure 5A). This suggests that AuNC treatment reduces neuron loss. In addition, the increased expression of GFAP and Iba-1in the OGD group (Figure 5B) is consistent with the activation of astrocytes and microglia in the cortex area. This change was less pronounced in the AuNC-treatment groups (Figure 5B), suggesting that AuNCs inhibited the activation of astrocytes and microglia in this stroke model.

It has been previously reported that nanoparticles can be selectively internalized by macrophages/microglia due to their inherent endocytic/phagocytic activity.[143,144] To determine whether this might be happening with AuNCs, we compared the biodistribution of AuNCs with that of microglia by multicolor labeling (Figure 5B), taking advantage of the physical properties of AuNCs which enable them to be used as imaging agents.[41,45,46] However, in the current study, AuNCs showed no apparent specific localization with microglia in the ex vivo stroke model, which might be due to the lack of blood circulation. Further investigations using in vivo models are required to understand the influence of AuNCs on different cell populations.

As AuNCs are bioimaging candidates for clinical diagnosis, the potential of AuNCs as theranostics for CNS disorders, especially those in which neuroinflammation is involved, also requires further investigation. L-NIBC protected AuNCs have recently been found to inhibit neuron loss in an animal model of Parkinson's disease,[52] and these data, in combination with our own, suggest that AuNCs may be useful therapeutic tools for neurodegenerative diseases such as Parkinson's disease and Alzheimer's disease. These data also raise the possibility that a AuNC-related neuronal protective role might not only be due to the bounded DHLA, as L-NIBC−AuNCs also showed similar beneficial effects.[52] Furthermore, the current study also provides a strategy for future material design to improve CNS regeneration, in which materials can be modified to incorporate immunomodulatory functions. Our in vitro data also imply that AuNCs alter the autophagy/apoptosis balance, another topic for future investigation.

In conclusion, our in vitro and ex vivo findings suggest that AuNCs effectively inhibit proinflammatory responses, possibly by inducing microglial polarization toward the tissue-regenerative M2-like phenotype (Scheme 1 in the Supporting Information). This polarization may benefit neural repair by inducing neurogenesis and axonal elongation while reducing astrogliosis. Therefore, we believe AuNCs deserve further attention as a strategy to manipulate the brain innate immune microenvironment to improve tissue regeneration in CNS. These agents could potentially be useful in treating acute CNS injuries such as stroke and other disorders involving neuroinflammation including Parkinson's disease and Alzheimer's disease.

METHODS

AuNC Preparation and Characterization. The synthesis of AuNCs was performed as previously described.[49] Briefly, 5.2 mg of DHLA was dissolved in 16 mL of an aqueous solution of NaOH (5 mM). After the solution was stirred for 5 min, 160 μL of $HAuCl_4$ (2%) was added to the DHLA mixture. Sodium borohydride (160 μL; 0.1 M) was then slowly added with vigorous stirring. The solution was then irradiated in a microwave oven for 4 min at 180 W. After microwave irradiation, the solution changed from a light yellow to a brownish color. After the solution cooled to room temperature, the AuNCs were purified using a 10 kDa Nanosep filter (Pall Nanosep, Ann Ann Arbor, MI). The brownish AuNCs were then loaded into dialysis bags with a MW cutoff of 12 kDa and placed into a 2 L large beaker filled with phosphate-buffered saline (PBS) overnight. Following dialysis, the purified AuNCs were stored at 4 °C for later use. AuNCs were then characterized by examining absorbance and fluorescence signals using a Biotek Synergy HT plate-reader and Xenogen IVIS Imaging System. The hydrodynamic diameters of AuNCs were measured by DLS.

Cell and Organotypic Brain Slice Culture. *BV2 Cells.* BV2 cells (a murine microglial cell line)[55,145,146] were used to investigate the effect of AuNCs on the microglial proinflammatory response. BV2 cells were cultured in Dulbecco's modified Eagle's medium (DMEM; Gibco, Thermo Fisher Scientific, Waltham, MA) with 10% fetal bovine serum (FBS; Lonza, Basel, Switzerland, heat-inactivated at 60 °C for over 30 min) and 1% (v/v) penicillin/streptomycin (P/S; Gibco, Thermo Fisher Scientific).

To simulate inflammatory conditions, BV2 cells were stimulated with 50 ng/mL LPS and IFNγ, along with

DOI: 10.1021/acs.nanolett.9b04216
Nano Lett. XXXX, XXX, XXX−XXX

AuNCs (1, 2, or 5 μg/mL and a vehicle control group treated with PBS) or the molar equivalent amount of DHLA. After that, cells were then washed with PBS before being incubated in serum-free DMEM for 12 h. The conditioned medium (CM) was harvested and subjected to centrifugation (1000*g*, 10 min, 4 °C), then filtered with a 0.2 μm filter (Millipore Corporation, Billerica, MA) to remove cell debris, and stored at −80 °C for future analysis.[147] The cells were washed with PBS and then harvested for further analysis. The IncuCyte ZOOM Live-Cell Analysis System (Essen BioScience, Ann Ann Arbor, MI) was used to monitor the real-time cell proliferation (percentage confluence) of BV2 cells. Data were analyzed using the IncuCyte software.

N2a Cells. N2a (Neuro2a cells—a murine neuroblastoma cell line) have been extensively used in neuronal differentiation and axonal growth studies.[128,148,149] N2a cells were expanded in DMEM with 10% FBS and 1% (v/v) P/S. Cells were cultured in incubators with 5% CO_2 at 37 °C to reach 80% confluence, after which they were passaged by treatment with 0.25% trypsin (containing 1 mM EDTA) for 2 min. The IncuCyte ZOOM Live-Cell Analysis System (Essen BioScience, Ann Ann Arbor, MI) was used to monitor the real-time cell proliferation (percentage confluence) of N2a cells.

To induce neuronal differentiation, N2a cells were treated with 20 μM retinoic acid (Sigma-Aldrich Pty. Ltd., Sydney, Australia) in DMEM supplemented with 2% FBS as previously described.[128,129] To study the effect of AuNC-treated BV2 cell-derived factors on neurogenesis, CM from BV2 cells (24 h stimulation with LPS and IFNγ) was mixed with DMEM containing 30 μM retinoic acid and 3% FBS at a 1:2 ratio. To investigate the effect of AuNCs on neuronal differentiation, N2a cells were also treated with AuNCs (1, 2, or 5 μg/mL and a vehicle control group treated with PBS) or the molar equivalent amount of DHLA. The IncuCyte ZOOM Live-Cell Analysis System (Essen BioScience, Ann Ann Arbor, MI) was used to monitor real-time cell morphological changes (eccentricity) during neuronal differentiation. The eccentricity was scored (ranged from 0 to 1) using IncuCyte software, where the eccentricity of cells with an elliptical shape is close to 1, while that of cells with a circular shape is 0. After 48 h, cells were harvested for further analysis. For measurement of neurite length, cells were observed and imaged with a light microscope and scored in a double-blind manner by two independent observers. For each group, six randomly selected images per well were used to quantify the average neurite length (per cell) using ImageJ software, and three wells were used for the calculations. All experiments were replicated three times.

Organotypic Brain Slice Model. To further analyze the effect of AuNCs, an ex vivo organotypic brain slice model was established as previously described.[150] Briefly, healthy brains were dissected from 4 week old C57BL/6 mice and then glued to the chuck of a water-cooled vibratome (NVSL Manual Vibroslice, World Precision Instruments, Hilton, Australia). The tissue was then sectioned into 400 μm whole brain slices (coronal plane), which were collected onto a membrane insert (Millicell-CM, Millipore) in culture medium. The whole procedure was performed under sterile conditions. Brain slices were then cultured in DMEM/HBSS medium with 25% heat-inactivated horse serum and 1% P/S (complete medium). PI staining was used to quantify cell death, and PI positivity was counted using a fluorescence microscope (EVOS FL Imaging System). All animal experiments were approved by the QIMR Berghofer Animal Ethics Committee (approval no. A0912609M).

To establish an ex vivo stroke model and simulate neuroinflammation, the brain slices were challenged with oxygen/glucose deprivation (OGD) as previously described.[135−137,151] The live brain slices were cultured in complete medium in an incubator with 5% CO_2 at 37 °C for 3 days. They were then switched to DMEM without glucose, and the environment was changed to 95% N_2 and 5% CO_2 for 20−30 min to induce OGD. They were reoxygenated and maintained in complete medium. The OGD-challenged brain slices were then treated with BV2 cell (24 h of stimulation with LPS and IFNγ)-derived CM mixed with DMEM/HBSS medium (containing 1% P/S) at a 1:2 ratio (then, heat-inactivated horse serum was added into the mixed medium to reach a concentration of 25%) to study the effect of AuNC-treated microglia on ex vivo neuronal regeneration. After 48 h of treatment, brain slices were harvested for protein analysis or fixed using 4% paraformaldehyde (PFA) in PBS (pH 7.4) for 6 h at room temperature.

To study the effect of AuNCs on ex vivo neuroinflammation, the OGD-challenged brain slices were treated with AuNCs (0, 2, or 5 μg/mL, 0 μg/mL served as OGD controls). The slices without OGD challenge served as normal controls (normal/healthy brain). After 48 h of treatment, the samples were fixed using 4% PFA.

MTT Assay and alamarBlue Cell Viability Assay. The MTT assay was used to evaluate the effects of AuNCs on the proliferation of BV2 and N2a cells as previously described.[152] Briefly, cells were seeded into 96-well plates (3000 cells/well, 3 wells/group) and treated with AuNCs (2, 5, 10, 30, or 60 μg/mL along with an untreated control group) in DMEM supplemented with 10% FBS and 1% P/S. After 24 h (BV2 cells) or 48 h (N2a cells), the culture medium was removed, and the cells were washed with PBS. Fresh culture medium (100 μL of DMEM with 10% FBS) containing MTT solution (0.5 mg/mL Sigma-Aldrich Pty Ltd.) was added to each well, and the plate was incubated at 37 °C for 4 h. The medium was then removed, and dimethyl sulfoxide (100 μL) was added into each well to solubilize the formazan product. The absorbance of each well was read at 570 nm by a SpectraMax Plus 384 plate-reader (Molecular Devices, LLC, San Jose, CA). The alamarBlue cell viability assay (Invitrogen, Thermo Fisher Scientific) was performed to examine the time-dependent metabolism changes in BV2 and N2a cells with a graded concentration of AuNCs, at every 24 h of culture for up to 72 h according to the manufacturer's protocol. After 72 h, cells were harvested for staining with trypan blue (0.4%, Invitrogen, Thermo Fisher Scientific) to determine cell life/death, and the cell survival rate was tested by the Countess II Automated Cell Counter (Countess, Thermo Fisher Scientific). Data were normalized against the control group. All experiments were replicated three times.

RNA Extraction, cDNA Synthesis, and Real-Time Quantitative-PCR (qPCR). Total RNA was extracted from BV2 cells using TRIzol Reagent (Ambion, Thermo Fisher Scientific, Waltham, MA). The cDNA was then synthesized from 1 μg of total RNA using the SensiFAST cDNA Synthesis Kit (Bioline Reagents, Meridian Bioscience Inc., Cincinnati, OH, USA) according to the manufacturer's instruction. Real-time polymerase chain reaction (qPCR) was performed by the QuantStudio 7 Flex Real-Time PCR System (Applied Biosystems, Thermo Fisher Scientific) with SYBR Green

DOI: 10.1021/acs.nanolett.9b04216
Nano Lett. XXXX, XXX, XXX−XXX

reagent (Applied Biosystems, Thermo Fisher Scientific)[147] to detect the mRNA levels of the following targets: *IL-1β*, *IL-6*, *MHC-II*, *TNF-α*, *CD86*, *iNOS*, *Arg-1*, *IL-10*, *TGF-β*, and *CD206*. The reference genes *Gapdh* and *Actb* were used as controls. Primer sequences are listed in Table 1 in the Supporting Information. Relative gene expression was normalized against *Gapdh* or *Actb* and calculated as previously described.[153] All experiments were following the MIQE guidelines[154] and replicated three times.

Protein Extraction and Western Blotting. The harvested cell samples (BV2 and N2a) and brain slices were homogenized in lysis buffer (20 mM HEPES (pH 7.4), 10% glycerol, 1% Triton X-100, 2 mM EDTA) containing cOmplete protease inhibitor cocktail (Roche, Dee Why, NSW, Australia). The BCA Protein Assay Kit (Thermo Fisher Scientific) was used to measure the protein concentration of the extracts according to the manufacturer's protocol. Western blotting was then performed as previously described.[147] Each sample (20 μg of protein) was loaded onto an SDS-PAGE gel (10% to 15%) and then separated and transferred to a nitrocellulose membrane (Merck Millipore, Billerica, MA). The membrane was blocked using Odyssey Blocking Buffer (LI-COR Biosciences, Lincoln, NE) for 1 h at room temperature and then incubated with primary antibodies against iNOS (1:250, Abcam, Cambridge, UK), NOX4 (1:1000, Abcam), NeuN (1:1500, Abcam), arginase (liver), NF-κB p100/52, Atg5, P62, LC3 A/B (1:1000, Cell Signaling Technology, Danvers, MA), Bcl-2 (1:500, Cell Signaling Technology, Danvers, MA), Bax (1:1000, Santa Cruz Biotechnology, Dallas, TX), nestin (1:250, Santa Cruz Biotechnology), caspase-3 (1:500, Genetex, Irvine, CA), GFAP (1:1000, Biocare Medical, Pacheco, CA); antibodies against α-tubulin (1:5000, Abcam) or β-actin (1:1000, Sigma-Aldrich Pty. Ltd.) were used as loading controls. After incubation at 4 °C overnight, the membranes were washed using tris-buffered saline (TBS) supplemented with 0.1% Tween 20 (TBST) and incubated with anti-rabbit IgG IRDye 800 conjugated secondary antibody (1:10000, Rockland, Gilbertsville) or anti-mouse IgG IRDye 700 conjugated secondary antibody (1:5000, Rockland) for 1 h at room temperature, washed with TBST. The membranes were then scanned/analyzed using an Odyssey Infrared Imaging System and Image Studio software (LI-COR Biosciences) according to the manufacturer's instructions. All antibodies were diluted in Odyssey Blocking Buffer. All experiments were replicated three times.

Enzyme-Linked Immunosorbent Assay. CM from BV2 cells was examined using enzyme-linked immunosorbent assays (ELISAs) to measure the concentration of secreted IL-1β, IL-6, TNF-α, and IL-10. Quantification of these cytokines was performed with the following kits according to the manufacturer's protocols: Mouse IL-1 beta/IL-1F2 Quantikine ELISA Kit; Mouse IL-6 Quantikine ELISA Kit; Mouse TNF-alpha Quantikine ELISA Kit; and Mouse IL-10 Quantikine ELISA Kit (R & D Systems, Minneapolis, MN). All experiments were replicated three times.

Reactive Oxygen Species (ROS) Detection. The cell-permeant molecule 2′,7′-dichlorodihydrofluorescein diacetate (H2DCFDA) was used for ROS detection in BV2 cells as previously described.[82−84] Briefly, BV2 cells (after 24 h of stimulation of LPS and IFNγ) were treated with prewarmed PBS containing 10 μM H2DCFDA (Sigma-Aldrich Pty. Ltd.) for 30 min in the incubator with 5% CO_2 at 37 °C. The cells were then washed with PBS and incubated in normal culture medium for a further 15 min before being detached using trypsin and resuspended in PBS. Flow cytometry was used to examine the fluorescent intensity (excitation: 485 nm; emission: 535 nm). Cells were protected from light during the entire process. All experiments were replicated three times.

Annexin V/7-AAD Assay and Annexin V/PI Staining. To detect cell apoptosis, the annexin V/7-AAD assay was performed[118−120] using the PE Annexin V Apoptosis Detection Kit I (BectonDickinson Labware, Franklin Lakes, NJ) according to the manufacturer's protocol.[117] Briefly, BV2 cells (after 24 h of stimulation) were detached using trypsin and resuspended in Binding Buffer (BectonDickinson Labware) at a concentration of 1×10^6 cells/mL. Cells were then incubated with PE−annexin V and 7-AAD for 15 min at room temperature (protected from light) before being analyzed by flow cytometry using a BD FACSVerse system (BectonDickinson Labware). Annexin V and 7-AAD double-negative cells were considered viable and nonapoptotic, while cells that were annexin V-positive and 7-AAD-negative were classified as in early apoptosis, and those that were annexin V and 7-AAD double-positive were considered in late apoptosis/dead.[117] For annexin V/PI staining, BV2 cells were seeded on a 96-well plate (100 000 cells per well) and stimulated for 24 h. After that, cells were washed by PBS and stained with FITC−annexin V and PI (BectonDickinson Labware) for 15 min at room temperature (protected from light) and then washed and read by the plate-reader (BMG Labtech, Ortenberg, Germany). All experiments were replicated three times.

H&E Staining. Fixed brain slices were dehydrated, embedded in paraffin, and then cut into 5 μm thick histologic sections. H&E staining was performed using a Leica Autostainer XL (ST5015, Leica Microsytem, North Ryde, Australia). One in every four sections was collected and analyzed by light microscopy.

Fluorescent Staining. *Monodansylcadaverine Staining.* The autofluorescent compound monodansylcadaverine (MDC) was used for detection of autophagic vacuoles in BV2 cells as previously described.[106−110] BV2 cells were seeded on 13 mm coverslips (ProSciTech, Kirwan, Australia) and treated with inflammatory stimuli and AuNCs as described above. Following treatment, cells were washed with PBS and fixed with 4% PFA for 20 min at room temperature. Cells were then washed with PBS and stained with 20 μM MDC dye (Sigma-Aldrich Pty. Ltd.) for 20 min at 37 °C in the dark. Cells were then washed with PBS and mounted with ProLong Gold antifade reagent with DAPI (Thermo Fisher Scientific, Waltham, MA, USA), secured to glass slides, and then observed using a Zeiss 780-NLO Point Scanning Confocal Microscope (ZEISS, North Ryde, Australia). All experiments were replicated three times.

Terminal Deoxynucleotidyl Transferase dUTP Nick End Labeling (TUNEL) Assay. TUNEL staining was used to detect BV2 cell apoptosis as previously described.[116] Briefly, BV2 cells (seeded on coverslips and treated with inflammatory stimuli and AuNCs for 24 h) were washed and fixed with 4% PFA and then stained using the TUNEL Apoptosis Detection Kit (Millipore Corporation, Billerica, MA, USA) following the manufacturer's instruction. The stained slices were observed using a Zeiss 780-NLO Point Scanning Confocal Microscope (ZEISS, North Ryde, Australia). The cells with positive-stained (green) nuclei were considered to be undergoing apoptosis. All experiments were replicated three times.

DOI: 10.1021/acs.nanolett.9b04216
Nano Lett. XXXX, XXX, XXX−XXX

Inmmunofluorescent Staining. Inmmunofluorescent staining was performed as previously described.[147] BV2 cells or N2a cells (seeded on 13 mm coverslips) were washed with PBS and fixed with 4% PFA for 20 min at room temperature. After washing, the samples were permeabilized by incubation with 0.2% Triton X-100 for 5 min at room temperature, washed with PBS, and then incubated with 2% BSA in PBS for 60 min at room temperature. The samples were then incubated with primary antibodies against either iNOS (1:200, abcam), CD206 (1:150, abcam), arginase (1:100, Abcam), NeuN (1:100, Abcam), or NF-κB p65 (1:300, Cell Signaling Technology), at 4 °C overnight. The samples were then washed with PBS and incubated with goat anti-rabbit Alexa Fluor 488 (1:1000, Cell Signaling Technology) secondary antibody for 30 min. All antibodies were diluted in 0.1% BSA in PBS. Samples were also stained with BODIPY 558/568 phalloidin (Thermo Fisher Scientific) for cytoskeleton detection. After washing, cells were mounted with ProLong Gold antifade reagent with DAPI (Thermo Fisher Scientific), secured to glass slides, and analyzed using a Nikon A1R Confocal Microscope (Nikon, Minato, Tokyo, Japan). All experiments were replicated three times.

For ex vivo tissue samples, sections were dewaxed, rehydrated, and washed using a Leica Autostainer XL. Antigen retrieval was performed by incubation with citrate retrieval buffer (Target Retrieval Solution, DAKO, Agilent Technologies, Santa Clara, CA), followed by microwaving for 2 min/150 W and then continuing to boil for 15 min. After cooling, the slides were washed in TBS and 0.025% Tween 20. The sections were then incubated with Biocare Medical Background Sniper in 2% bovine serum albumin (BSA, diluted in PBS, Sigma-Aldrich Pty. Ltd.) for 10 min. After the blocking solution was aspirated, the sections were incubated for 30 min at room temperature with primary antibodies against NeuN (1:7500, Abcam), GFAP (1:20 000, Biocare Medical), or Iba-1 (1:6000, Abcam). Sections were then washed and incubated with goat anti-mouse Alexa Fluor 568 (1:1000, Thermo Fisher Scientific), goat anti-rabbit Alexa Fluor 488 (1:1000, Cell Signaling Technology), and donkey anti-mouse Alexa Fluor 647 (1:1000, Thermo Fisher Scientific) secondary antibodies for 30 min. Nuclei were stained with DAPI. Finally, the sections were washed with PBS, mounted, and viewed using a Zeiss 780-NLO Point Scanning Confocal Microscope (ZEISS). All experiments were replicated three times.

Statistical Analysis. Student's *t* tests were performed for comparison between two groups. For comparison in multiple groups, data were subjected to one-way ANOVA followed by the Student–Newman–Keul test at $\alpha = 0.05$. $P < 0.05$ was considered to be significantly different. The data were analyzed using SPSS 13.0 (SPSS Inc., Chicago, IL).

■ ASSOCIATED CONTENT

Supporting Information

The Supporting Information is available free of charge at https://pubs.acs.org/doi/10.1021/acs.nanolett.9b04216.

Table 1, supplementary figures, and Scheme 1 (PDF)

■ AUTHOR INFORMATION

Corresponding Authors

*E-mail: michelle.liu@qimrberghofer.edu.au. (T.L.)
*E-mail: yin.xiao@qut.edu.au. (Y.X.)

ORCID

Lan Xiao: 0000-0002-5227-9352

Notes

The authors declare no competing financial interest.

■ ACKNOWLEDGMENTS

Dr. Tianqing Liu is supported by the National Health and Medical Research Council (NHMRC) Early Career Fellowship (Grant No. 1112258). Dr. Yinghong Zhou is supported by the National Health and Medical Research Council (NHMRC) Early Career Fellowship (Grant No. 1105035).

■ REFERENCES

(1) Ramlackhansingh, A. F.; Brooks, D. J.; Greenwood, R. J.; Bose, S. K.; Turkheimer, F. E.; Kinnunen, K. M.; Gentleman, S.; Heckemann, R. A.; Gunanayagam, K.; Gelosa, G.; et al. Inflammation after trauma: microglial activation and traumatic brain injury. *Ann. Neurol.* **2011**, *70* (3), 374–383.

(2) Perry, V. H.; Nicoll, J. A.; Holmes, C. Microglia in neurodegenerative disease. *Nat. Rev. Neurol.* **2010**, *6* (4), 193.

(3) Liesz, A.; Zhou, W.; Mracsko, E.; Karcher, S.; Bauer, H.; Schwarting, S.; Sun, L.; Bruder, D.; Stegemann, S.; Cerwenka, A.; et al. Inhibition of lymphocyte trafficking shields the brain against deleterious neuroinflammation after stroke. *Brain* **2011**, *134* (3), 704–720.

(4) Fan, L.-W.; Pang, Y. Dysregulation of neurogenesis by neuroinflammation: key differences in neurodevelopmental and neurological disorders. *Neural Regener. Res.* **2017**, *12* (3), 366.

(5) Smith, J. A.; Das, A.; Ray, S. K.; Banik, N. L. Role of pro-inflammatory cytokines released from microglia in neurodegenerative diseases. *Brain Res. Bull.* **2012**, *87* (1), 10–20.

(6) Streit, W. J.; Mrak, R. E.; Griffin, W. S. T. Microglia and neuroinflammation: a pathological perspective. *J. Neuroinflammation* **2004**, *1* (1), 14.

(7) Lehnardt, S. Innate immunity and neuroinflammation in the CNS: The role of microglia in Toll-like receptor-mediated neuronal injury. *Glia* **2010**, *58* (3), 253–263.

(8) Hu, X.; Leak, R. K.; Shi, Y.; Suenaga, J.; Gao, Y.; Zheng, P.; Chen, J. Microglial and macrophage polarization—new prospects for brain repair. *Nat. Rev. Neurol.* **2015**, *11* (1), 56.

(9) Colton, C. A.; Wilcock, D. M. Assessing activation states in microglia. *CNS Neurol. Disord.: Drug Targets* **2010**, *9* (2), 174–191.

(10) Colton, C. A. Heterogeneity of microglial activation in the innate immune response in the brain. *J. Neuroimmune Pharmacol.* **2009**, *4* (4), 399–418.

(11) Ponomarev, E. D.; Maresz, K.; Tan, Y.; Dittel, B. N. CNS-derived interleukin-4 is essential for the regulation of autoimmune inflammation and induces a state of alternative activation in microglial cells. *J. Neurosci.* **2007**, *27* (40), 10714–10721.

(12) Yang, X.; Xu, S.; Qian, Y.; Xiao, Q. Resveratrol regulates microglia M1/M2 polarization via PGC-1α in conditions of neuroinflammatory injury. *Brain, Behav., Immun.* **2017**, *64*, 162–172.

(13) Block, M. L.; Zecca, L.; Hong, J.-S. Microglia-mediated neurotoxicity: uncovering the molecular mechanisms. *Nat. Rev. Neurosci.* **2007**, *8* (1), 57.

(14) Prinz, M.; Priller, J. Microglia and brain macrophages in the molecular age: from origin to neuropsychiatric disease. *Nat. Rev. Neurosci.* **2014**, *15* (5), 300.

(15) Jacque, C.; Vinner, C.; Kujas, M.; Raoul, M.; Racadot, J.; Baumann, N. Determination of glial fibrillary acidic protein (GFAP) in human brain tumors. *J. Neurol. Sci.* **1978**, *35* (1), 147–155.

(16) Pekny, M.; Nilsson, M. Astrocyte activation and reactive gliosis. *Glia* **2005**, *50* (4), 427–434.

(17) Sofroniew, M. V. Molecular dissection of reactive astrogliosis and glial scar formation. *Trends Neurosci.* **2009**, *32* (12), 638–647.

DOI: 10.1021/acs.nanolett.9b04216
Nano Lett. XXXX, XXX, XXX–XXX

(18) Colonna, M.; Butovsky, O. Microglia function in the central nervous system during health and neurodegeneration. *Annu. Rev. Immunol.* **2017**, *35*, 441−468.
(19) Belarbi, K.; Rosi, S. Modulation of adult-born neurons in the inflamed hippocampus. *Front. Cell. Neurosci.* **2013**, *7*, 145.
(20) Shahsavari, S.; Behroozi, F. Gold Nanoclusters: Nanomedicine Potentials and Applications. *J. Nanomed Res.* **2016**, *3* (5), No. 00069.
(21) Hu, X.; Li, P.; Guo, Y.; Wang, H.; Leak, R. K.; Chen, S.; Gao, Y.; Chen, J. Microglia/macrophage polarization dynamics reveal novel mechanism of injury expansion after focal cerebral ischemia. *Stroke* **2012**, *43* (11), 3063−3070.
(22) Tang, Y.; Le, W. Differential roles of M1 and M2 microglia in neurodegenerative diseases. *Mol. Neurobiol.* **2016**, *53* (2), 1181−1194.
(23) Hall, E. D. Lipid antioxidants in acute central nervous system injury. *Ann. Emerg. Med.* **1993**, *22* (6), 1022−1027.
(24) Leu, J.-G.; Chen, S.-A.; Chen, H.-M.; Wu, W.-M.; Hung, C.-F.; Yao, Y.-D.; Tu, C.-S.; Liang, Y.-J. The effects of gold nanoparticles in wound healing with antioxidant epigallocatechin gallate and α-lipoic acid. *Nanomedicine* **2012**, *8* (5), 767−775.
(25) Packer, L.; Tritschler, H. J.; Wessel, K. Neuroprotection by the metabolic antioxidant α-lipoic acid. *Free Radical Biol. Med.* **1997**, *22* (1−2), 359−378.
(26) Maczurek, A.; Hager, K.; Kenklies, M.; Sharman, M.; Martins, R.; Engel, J.; Carlson, D. A.; Münch, G. Lipoic acid as an anti-inflammatory and neuroprotective treatment for Alzheimer's disease. *Adv. Drug Delivery Rev.* **2008**, *60* (13−14), 1463−1470.
(27) Ghibu, S.; Richard, C.; Vergely, C.; Zeller, M.; Cottin, Y.; Rochette, L. Antioxidant properties of an endogenous thiol: alpha-lipoic acid, useful in the prevention of cardiovascular diseases. *J. Cardiovasc. Pharmacol.* **2009**, *54* (5), 391−398.
(28) Bustamante, J.; Lodge, J. K.; Marcocci, L.; Tritschler, H. J.; Packer, L.; Rihn, B. H. α-Lipoic acid in liver metabolism and disease. *Free Radical Biol. Med.* **1998**, *24* (6), 1023−1039.
(29) Shinto, L.; Quinn, J.; Montine, T.; Dodge, H. H.; Woodward, W.; Baldauf-Wagner, S.; Waichunas, D.; Bumgarner, L.; Bourdette, D.; Silbert, L.; et al. A randomized placebo-controlled pilot trial of omega-3 fatty acids and alpha lipoic acid in Alzheimer's disease. *J. Alzheimer's Dis.* **2013**, *38* (1), 111−120.
(30) Kamenova, P. Improvement of insulin sensitivity in patients with type 2 diabetes mellitus after oral administration of alpha-lipoic acid. *HORMONES-ATHENS-* **2006**, *5* (4), 251.
(31) Paradells-Navarro, S.; Benlloch-Navarro, M. S.; Almansa Frias, M. a. I.; Garcia-Esparza, M. A.; Broccoli, V.; Miranda, M.; Soria, J. M. Neuroprotection of brain cells by lipoic acid treatment after cellular stress. *ACS Chem. Neurosci.* **2017**, *8* (3), 569−577.
(32) Gorąca, A.; Huk-Kolega, H.; Piechota, A.; Kleniewska, P.; Ciejka, E.; Skibska, B. Lipoic acid−biological activity and therapeutic potential. *Pharmacol. Rep.* **2011**, *63* (4), 849−858.
(33) Çakatay, U. Pro-oxidant actions of α-lipoic acid and dihydrolipoic acid. *Med. Hypotheses* **2006**, *66* (1), 110−117.
(34) Biewenga, G. P.; Haenen, G. R.; Bast, A. The pharmacology of the antioxidant lipoic acid. *Gen. Pharmacol.* **1997**, *29* (3), 315−331.
(35) Moini, H.; Packer, L.; Saris, N.-E. L. Antioxidant and prooxidant activities of α-lipoic acid and dihydrolipoic acid. *Toxicol. Appl. Pharmacol.* **2002**, *182* (1), 84−90.
(36) Ho, Y.-S.; Lai, C.-S.; Liu, H.-I.; Ho, S.-Y.; Tai, C.; Pan, M.-H.; Wang, Y.-J. Dihydrolipoic acid inhibits skin tumor promotion through anti-inflammation and anti-oxidation. *Biochem. Pharmacol.* **2007**, *73* (11), 1786−1795.
(37) Greenamyre, J. T.; Garcia-Osuna, M.; Greene, J. G. The endogenous cofactors, thioctic acid and dihydrolipoic acid, are neuroprotective against NMDA and malonic acid lesions of striatum. *Neurosci. Lett.* **1994**, *171* (1−2), 17−20.
(38) Koenig, M. L.; Meyerhoff, J. L. In vitro neuroprotection against oxidative stress by pre-treatment with a combination of dihydrolipoic acid and phenyl-butyl nitrones. *Neurotoxic. Res.* **2003**, *5* (4), 265−272.
(39) Zhou, K.; Enkhjargal, B.; Xie, Z.; Sun, C.; Wu, L.; Malaguit, J.; Chen, S.; Tang, J.; Zhang, J.; Zhang, J. H. Dihydrolipoic acid inhibits lysosomal rupture and NLRP3 through lysosome-associated membrane protein-1/calcium/calmodulin-dependent protein kinase II/TAK1 pathways after subarachnoid hemorrhage in rat. *Stroke* **2018**, *49* (1), 175−183.
(40) Dobrovolskaia, M. A.; Mcneil, S. E. Immunological properties of engineered nanomaterials. *Nat. Nanotechnol.* **2007**, *2* (8), 469−478.
(41) Bhaskar, S.; Tian, F.; Stoeger, T.; Kreyling, W.; de la Fuente, J. M.; Grazú, V.; Borm, P.; Estrada, G.; Ntziachristos, V.; Razansky, D. Multifunctional Nanocarriers for diagnostics, drug delivery and targeted treatment across blood-brain barrier: perspectives on tracking and neuroimaging. *Part. Fibre Toxicol.* **2010**, *7* (1), 3.
(42) Zhao, Y.; Detering, L.; Sultan, D.; Cooper, M. L.; You, M.; Cho, S.; Meier, S. L.; Luehmann, H.; Sun, G.; Rettig, M.; et al. Gold nanoclusters doped with 64Cu for CXCR4 positron emission tomography imaging of breast cancer and metastasis. *ACS Nano* **2016**, *10* (6), 5959−5970.
(43) Zheng, Y.; Lai, L.; Liu, W.; Jiang, H.; Wang, X. Recent advances in biomedical applications of fluorescent gold nanoclusters. *Adv. Colloid Interface Sci.* **2017**, *242*, 1−16.
(44) Li, J.; Zhu, J.-J.; Xu, K. Fluorescent metal nanoclusters: from synthesis to applications. *TrAC, Trends Anal. Chem.* **2014**, *58*, 90−98.
(45) Zhang, L.; Wang, E. Metal nanoclusters: new fluorescent probes for sensors and bioimaging. *Nano Today* **2014**, *9* (1), 132−157.
(46) Zhang, C.; Zhou, Z.; Qian, Q.; Gao, G.; Li, C.; Feng, L.; Wang, Q.; Cui, D. Glutathione-capped fluorescent gold nanoclusters for dual-modal fluorescence/X-ray computed tomography imaging. *J. Mater. Chem. B* **2013**, *1* (38), 5045−5053.
(47) Nair, L. V.; Nair, R. V.; Shenoy, S. J.; Thekkuveettil, A.; Jayasree, R. S. Blood brain barrier permeable gold nanocluster for targeted brain imaging and therapy: an in vitro and in vivo study. *J. Mater. Chem. B* **2017**, *5* (42), 8314.
(48) Fernández, T. D.; Pearson, J. R.; Leal, M. P.; Torres, M. J.; Blanca, M.; Mayorga, C.; Le Guével, X. Intracellular accumulation and immunological properties of fluorescent gold nanoclusters in human dendritic cells. *Biomaterials* **2015**, *43*, 1−12.
(49) Shang, L.; Yang, L.; Stockmar, F.; Popescu, R.; Trouillet, V.; Bruns, M.; Gerthsen, D.; Nienhaus, G. U. Microwave-assisted rapid synthesis of luminescent gold nanoclusters for sensing Hg 2+ in living cells using fluorescence imaging. *Nanoscale* **2012**, *4* (14), 4155−4160.
(50) Nair, L. V.; Nazeer, S. S.; Jayasree, R. S.; Ajayaghosh, A. Fluorescence imaging assisted photodynamic therapy using photosensitizer-linked gold quantum clusters. *ACS Nano* **2015**, *9* (6), 5825−5832.
(51) Song, X.-R.; Goswami, N.; Yang, H.-H.; Xie, J. Functionalization of metal nanoclusters for biomedical applications. *Analyst* **2016**, *141* (11), 3126−3140.
(52) Gao, G.; Chen, R.; He, M.; Li, J.; Li, J.; Wang, L.; Sun, T. Gold nanoclusters for Parkinson's disease treatment. *Biomaterials* **2019**, *194*, 36−46.
(53) Shang, L.; Stockmar, F.; Azadfar, N.; Nienhaus, G. U. Intracellular thermometry by using fluorescent gold nanoclusters. *Angew. Chem., Int. Ed.* **2013**, *52* (42), 11154−11157.
(54) Shang, L.; Azadfar, N.; Stockmar, F.; Send, W.; Trouillet, V.; Bruns, M.; Gerthsen, D.; Nienhaus, G. U. One-Pot Synthesis of Near-Infrared Fluorescent Gold Clusters for Cellular Fluorescence Lifetime Imaging. *Small* **2011**, *7* (18), 2614−2620.
(55) Henn, A.; Lund, S.; Hedtjärn, M.; Schrattenholz, A.; Pörzgen, P.; Leist, M. The suitability of BV2 cells as alternative model system for primary microglia cultures or for animal experiments examining brain inflammation. *ALTEX-Alternatives to animal experimentation* **2009**, *26* (2), 83−94.
(56) Bae, E.-A.; Kim, E.-J.; Park, J.-S.; Kim, H.-S.; Ryu, J. H.; Kim, D.-H. Ginsenosides Rg3 and Rh2 inhibit the activation of AP-1 and protein kinase A pathway in lipopolysaccharide/interferon-γ-stimulated BV-2 microglial cells. *Planta Med.* **2006**, *72* (07), 627−633.
(57) Moss, D. W.; Bates, T. E. Activation of murine microglial cell lines by lipopolysaccharide and interferon-γ causes NO-mediated decreases in mitochondrial and cellular function. *Eur. J. Neurosci.* **2001**, *13* (3), 529−538.

DOI: 10.1021/acs.nanolett.9b04216
Nano Lett. XXXX, XXX, XXX−XXX

(58) Guillemin, G. J.; Brew, B. J. Microglia, macrophages, perivascular macrophages, and pericytes: a review of function and identification. *J. Leukocyte Biol.* **2004**, *75* (3), 388−397.
(59) Chhor, V.; Le Charpentier, T.; Lebon, S.; Oré, M.-V.; Celador, I. L.; Josserand, J.; Degos, V.; Jacotot, E.; Hagberg, H.; Sävman, K.; et al. Characterization of phenotype markers and neuronotoxic potential of polarised primary microglia in vitro. *Brain, Behav., Immun.* **2013**, *32*, 70−85.
(60) Gosselin, D.; Rivest, S. Role of IL-1 and TNF in the brain: twenty years of progress on a Dr. Jekyll/Mr. Hyde duality of the innate immune system. *Brain, Behav., Immun.* **2007**, *21* (3), 281−289.
(61) Gloor, S. M.; Wachtel, M.; Bolliger, M. F.; Ishihara, H.; Landmann, R.; Frei, K. Molecular and cellular permeability control at the blood−brain barrier. *Brain Res. Rev.* **2001**, *36* (2−3), 258−264.
(62) Zhao, C.; Ling, Z.; Newman, M. B.; Bhatia, A.; Carvey, P. M. TNF-α knockout and minocycline treatment attenuates blood−brain barrier leakage in MPTP-treated mice. *Neurobiol. Dis.* **2007**, *26* (1), 36−46.
(63) Erta, M.; Quintana, A.; Hidalgo, J. Interleukin-6, a major cytokine in the central nervous system. *Int. J. Biol. Sci.* **2012**, *8* (9), 1254.
(64) Lipton, S. A.; Choi, Y.-B.; Pan, Z.-H.; Lei, S. Z.; Chen, H.-S. V.; Sucher, N. J.; Loscalzo, J.; Singel, D. J.; Stamler, J. S. A redox-based mechanism for the neuroprotective and neurodestructive effects of nitric oxide and related nitroso-compounds. *Nature* **1993**, *364* (6438), 626.
(65) Dawson, V. L.; Dawson, T.; Bartley, D.; Uhl, G.; Snyder, S. Mechanisms of nitric oxide-mediated neurotoxicity in primary brain cultures. *J. Neurosci.* **1993**, *13* (6), 2651−2661.
(66) Chao, C.; Hu, S.; Molitor, T.; Shaskan, E.; Peterson, P. Activated microglia mediate neuronal cell injury via a nitric oxide mechanism. *J. Immunol.* **1992**, *149* (8), 2736−2741.
(67) Butovsky, O.; Ziv, Y.; Schwartz, A.; Landa, G.; Talpalar, A. E.; Pluchino, S.; Martino, G.; Schwartz, M. Microglia activated by IL-4 or IFN-γ differentially induce neurogenesis and oligodendrogenesis from adult stem/progenitor cells. *Mol. Cell. Neurosci.* **2006**, *31* (1), 149−160.
(68) Kaltschmidt, C.; Kaltschmidt, B.; Lannes-Vieira, J.; Kreutzberg, G. W.; Wekerle, H.; Baeuerle, P. A.; Gehrmann, J. Transcription factor NF-κB is activated in microglia during experimental autoimmune encephalomyelitis. *J. Neuroimmunol.* **1994**, *55* (1), 99−106.
(69) Ryu, J.; Pyo, H.; Jou, I.; Joe, E. Thrombin induces NO release from cultured rat microglia via protein kinase C, mitogen-activated protein kinase, and NF-κB. *J. Biol. Chem.* **2000**, *275* (39), 29955−29959.
(70) Kim, Y. J.; Hwang, S. Y.; Oh, E. S.; Oh, S.; Han, I. O. IL-1β, an immediate early protein secreted by activated microglia, induces iNOS/NO in C6 astrocytoma cells through p38 MAPK and NF-κB pathways. *J. Neurosci. Res.* **2006**, *84* (5), 1037−1046.
(71) Lawrence, T. The nuclear factor NF-κB pathway in inflammation. *Cold Spring Harbor Perspect. Biol.* **2009**, *1*, a001651.
(72) Ten, R.; Paya, C.; Israel, N.; Le Bail, O.; Mattei, M.; Virelizier, J.; Kourilsky, P.; Israel, A. The characterization of the promoter of the gene encoding the p50 subunit of NF-kappa B indicates that it participates in its own regulation. *EMBO J.* **1992**, *11* (1), 195−203.
(73) Flohé, L.; Brigelius-Flohé, R.; Saliou, C.; Traber, M. G.; Packer, L. Redox regulation of NF-kappa B activation. *Free Radical Biol. Med.* **1997**, *22* (6), 1115−1126.
(74) Park, J.; Min, J.-S.; Kim, B.; Chae, U.-B.; Yun, J. W.; Choi, M.-S.; Kong, I.-K.; Chang, K.-T.; Lee, D.-S. Mitochondrial ROS govern the LPS-induced pro-inflammatory response in microglia cells by regulating MAPK and NF-κB pathways. *Neurosci. Lett.* **2015**, *584*, 191−196.
(75) Forrester, S. J.; Kikuchi, D. S.; Hernandes, M. S.; Xu, Q.; Griendling, K. K. Reactive oxygen species in metabolic and inflammatory signaling. *Circ. Res.* **2018**, *122* (6), 877−902.
(76) Lin, M. T.; Beal, M. F. Mitochondrial dysfunction and oxidative stress in neurodegenerative diseases. *Nature* **2006**, *443* (7113), 787.
(77) Allen, C. L.; Bayraktutan, U. Oxidative stress and its role in the pathogenesis of ischaemic stroke. *Int. J. Stroke* **2009**, *4* (6), 461−470.
(78) Singh, I. N.; Sullivan, P. G.; Deng, Y.; Mbye, L. H.; Hall, E. D. Time course of post-traumatic mitochondrial oxidative damage and dysfunction in a mouse model of focal traumatic brain injury: implications for neuroprotective therapy. *J. Cereb. Blood Flow Metab.* **2006**, *26* (11), 1407−1418.
(79) Mittal, M.; Siddiqui, M. R.; Tran, K.; Reddy, S. P.; Malik, A. B. Reactive oxygen species in inflammation and tissue injury. *Antioxid. Redox Signaling* **2014**, *20* (7), 1126−1167.
(80) Morgan, M. J.; Liu, Z.-g. Crosstalk of reactive oxygen species and NF-κB signaling. *Cell Res.* **2011**, *21* (1), 103.
(81) Gloire, G.; Legrand-Poels, S.; Piette, J. NF-κB activation by reactive oxygen species: fifteen years later. *Biochem. Pharmacol.* **2006**, *72* (11), 1493−1505.
(82) Myhre, O.; Andersen, J. M.; Aarnes, H.; Fonnum, F. Evaluation of the probes 2′, 7′-dichlorofluorescin diacetate, luminol, and lucigenin as indicators of reactive species formation. *Biochem. Pharmacol.* **2003**, *65* (10), 1575−1582.
(83) LeBel, C. P.; Ischiropoulos, H.; Bondy, S. C. Evaluation of the probe 2', 7'-dichlorofluorescin as an indicator of reactive oxygen species formation and oxidative stress. *Chem. Res. Toxicol.* **1992**, *5* (2), 227−231.
(84) Royall, J. A.; Ischiropoulos, H. Evaluation of 2′, 7′-dichlorofluorescin and dihydrorhodamine 123 as fluorescent probes for intracellular H2O2 in cultured endothelial cells. *Arch. Biochem. Biophys.* **1993**, *302* (2), 348−355.
(85) Yuan, L.; Wu, Y.; Ren, X.; Liu, Q.; Wang, J.; Liu, X. Isoorientin attenuates lipopolysaccharide-induced pro-inflammatory responses through down-regulation of ROS-related MAPK/NF-κB signaling pathway in BV-2 microglia. *Mol. Cell. Biochem.* **2014**, *386* (1−2), 153−165.
(86) Kuroda, J.; Ago, T.; Matsushima, S.; Zhai, P.; Schneider, M. D.; Sadoshima, J. NADPH oxidase 4 (Nox4) is a major source of oxidative stress in the failing heart. *Proc. Natl. Acad. Sci. U. S. A.* **2010**, *107* (35), 15565−15570.
(87) Wu, D.-C.; Teismann, P.; Tieu, K.; Vila, M.; Jackson-Lewis, V.; Ischiropoulos, H.; Przedborski, S. NADPH oxidase mediates oxidative stress in the 1-methyl-4-phenyl-1, 2, 3, 6-tetrahydropyridine model of Parkinson's disease. *Proc. Natl. Acad. Sci. U. S. A.* **2003**, *100* (10), 6145−6150.
(88) Chen, K.; Kirber, M. T.; Xiao, H.; Yang, Y.; Keaney, J. F. Regulation of ROS signal transduction by NADPH oxidase 4 localization. *J. Cell Biol.* **2008**, *181* (7), 1129−1139.
(89) Sirokmány, G.; Donkó, Á.; Geiszt, M. Nox/Duox family of NADPH oxidases: lessons from knockout mouse models. *Trends Pharmacol. Sci.* **2016**, *37* (4), 318−327.
(90) Maiuri, M. C.; Zalckvar, E.; Kimchi, A.; Kroemer, G. Self-eating and self-killing: crosstalk between autophagy and apoptosis. *Nat. Rev. Mol. Cell Biol.* **2007**, *8* (9), 741.
(91) Shaid, S.; Brandts, C.; Serve, H.; Dikic, I. Ubiquitination and selective autophagy. *Cell Death Differ.* **2013**, *20* (1), 21.
(92) Zhong, Z.; Sanchez-Lopez, E.; Karin, M. Autophagy, inflammation, and immunity: a troika governing cancer and its treatment. *Cell* **2016**, *166* (2), 288−298.
(93) Li, Q.; Barres, B. A. Microglia and macrophages in brain homeostasis and disease. *Nat. Rev. Immunol.* **2018**, *18* (4), 225.
(94) Vidal, P.; Lemmens, E.; Avila, A.; Vangansewinkel, T.; Chalaris, A.; Rose-John, S.; Hendrix, S. ADAM17 is a survival factor for microglial cells in vitro and in vivo after spinal cord injury in mice. *Cell Death Dis.* **2013**, *4* (12), e954.
(95) Wei, Z.; Yu, D.; Bi, Y.; Cao, Y. A disintegrin and metalloprotease 17 promotes microglial cell survival via epidermal growth factor receptor signalling following spinal cord injury. *Mol. Med. Rep.* **2015**, *12* (1), 63−70.
(96) Yang, Z.; Klionsky, D. J. Mammalian autophagy: core molecular machinery and signaling regulation. *Curr. Opin. Cell Biol.* **2010**, *22* (2), 124−131.

DOI: 10.1021/acs.nanolett.9b04216
Nano Lett. XXXX, XXX, XXX−XXX

(97) Mizushima, N.; Komatsu, M. Autophagy: renovation of cells and tissues. *Cell* **2011**, *147* (4), 728−741.
(98) Zhong, Z.; Umemura, A.; Sanchez-Lopez, E.; Liang, S.; Shalapour, S.; Wong, J.; He, F.; Boassa, D.; Perkins, G.; Ali, S. R.; et al. NF-κB restricts inflammasome activation via elimination of damaged mitochondria. *Cell* **2016**, *164* (5), 896−910.
(99) Shi, J.; Wong, J.; Piesik, P.; Fung, G.; Zhang, J.; Jagdeo, J.; Li, X.; Jan, E.; Luo, H. Cleavage of sequestosome 1/p62 by an enteroviral protease results in disrupted selective autophagy and impaired NFKB signaling. *Autophagy* **2013**, *9* (10), 1591−1603.
(100) Elliott, E. I.; Sutterwala, F. S. Initiation and perpetuation of NLRP 3 inflammasome activation and assembly. *Immunol. Rev.* **2015**, *265* (1), 35−52.
(101) Zhou, R.; Yazdi, A. S.; Menu, P.; Tschopp, J. A role for mitochondria in NLRP3 inflammasome activation. *Nature* **2011**, *469* (7329), 221.
(102) Sun, Q.; Fan, J.; Billiar, T. R.; Scott, M. J. Inflammasome and autophagy regulation: a two-way street. *Mol. Med.* **2017**, *23*, 188.
(103) Kroemer, G.; Levine, B. Autophagic cell death: the story of a misnomer. *Nat. Rev. Mol. Cell Biol.* **2008**, *9* (12), 1004.
(104) Liu, Y.; Shoji-Kawata, S.; Sumpter, R. M.; Wei, Y.; Ginet, V.; Zhang, L.; Posner, B.; Tran, K. A.; Green, D. R.; Xavier, R. J.; et al. Autosis is a Na+, K+-ATPase−regulated form of cell death triggered by autophagy-inducing peptides, starvation, and hypoxia−ischemia. *Proc. Natl. Acad. Sci. U. S. A.* **2013**, *110* (51), 20364−20371.
(105) Liu, Y.; Levine, B. Autosis and autophagic cell death: the dark side of autophagy. *Cell Death Differ.* **2015**, *22* (3), 367.
(106) Biederbick, A.; Kern, H. F.; Elsässer, H. Monodansylcadaverine (MDC) is a specific in vivo marker for autophagic vacuoles. *Eur. J. Cell Biol.* **1995**, *66* (1), 3−14.
(107) Singh, S. B.; Davis, A. S.; Taylor, G. A.; Deretic, V. Human IRGM induces autophagy to eliminate intracellular mycobacteria. *Science* **2006**, *313* (5792), 1438−1441.
(108) Vazquez, C. L.; Colombo, M. I. Assays to assess autophagy induction and fusion of autophagic vacuoles with a degradative compartment, using monodansylcadaverine (MDC) and DQ-BSA. *Methods Enzymol.* **2009**, *452*, 85−95.
(109) Klionsky, D. J.; Abdelmohsen, K.; Abe, A.; Abedin, M. J.; Abeliovich, H.; Acevedo Arozena, A.; Adachi, H.; Adams, C. M.; Adams, P. D.; Adeli, K.; et al. Guidelines for the use and interpretation of assays for monitoring autophagy. *Autophagy* **2016**, *12* (1), 1−222.
(110) Niemann, A.; Baltes, J.; Elsässer, H.-P. Fluorescence properties and staining behavior of monodansylpentane, a structural homologue of the lysosomotropic agent monodansylcadaverine. *J. Histochem. Cytochem.* **2001**, *49* (2), 177−185.
(111) Kabeya, Y.; Mizushima, N.; Ueno, T.; Yamamoto, A.; Kirisako, T.; Noda, T.; Kominami, E.; Ohsumi, Y.; Yoshimori, T. LC3, a mammalian homologue of yeast Apg8p, is localized in autophagosome membranes after processing. *EMBO journal* **2000**, *19* (21), 5720−5728.
(112) Kabeya, Y.; Mizushima, N.; Yamamoto, A.; Oshitani-Okamoto, S.; Ohsumi, Y.; Yoshimori, T. LC3, GABARAP and GATE16 localize to autophagosomal membrane depending on form-II formation. *J. Cell Sci.* **2004**, *117* (13), 2805−2812.
(113) Klionsky, D. J.; Cuervo, A. M.; Seglen, P. O. Methods for monitoring autophagy from yeast to human. *Autophagy* **2007**, *3* (3), 181−206.
(114) Mizushima, N.; Yoshimori, T. How to interpret LC3 immunoblotting. *Autophagy* **2007**, *3* (6), 542−545.
(115) Bjørkøy, G.; Lamark, T.; Pankiv, S.; Øvervatn, A.; Brech, A.; Johansen, T. Monitoring autophagic degradation of p62/SQSTM1. *Methods Enzymol.* **2009**, *452*, 181−197.
(116) Gorczyca, W.; Traganos, F.; Jesionowska, H.; Darzynkiewicz, Z. Presence of DNA strand breaks and increased sensitivity of DNA in situ to denaturation in abnormal human sperm cells: analogy to apoptosis of somatic cells. *Exp. Cell Res.* **1993**, *207* (1), 202−205.
(117) Hingorani, R.; Deng, J.; Elia, J.; McIntyre, C.; Mittar, D. *Detection of apoptosis using the BD Annexin V FITC Assay on the BD FACSVerse System*; Application Note; BD Biosciences, 2011.
(118) Ishaque, A.; Al-Rubeai, M. Use of intracellular pH and annexin-V flow cytometric assays to monitor apoptosis and its suppression by bcl-2 over-expression in hybridoma cell culture. *J. Immunol. Methods* **1998**, *221* (1−2), 43−57.
(119) Vermes, I.; Haanen, C.; Steffens-Nakken, H.; Reutellingsperger, C. A novel assay for apoptosis flow cytometric detection of phosphatidylserine expression on early apoptotic cells using fluorescein labelled annexin V. *J. Immunol. Methods* **1995**, *184* (1), 39−51.
(120) Dachary-Prigent, J.; Freyssinet, J.-M.; Pasquet, J.-M.; Carron, J.-C.; Nurden, A. T. Annexin V as a probe of aminophospholipid exposure and platelet membrane vesiculation: a flow cytometry study showing a role for free sulfhydryl groups. *Blood* **1993**, *81* (10), 2554−2565.
(121) Bundscherer, A.; Malsy, M.; Lange, R.; Hofmann, P.; Metterlein, T.; Graf, B. M.; Gruber, M. Cell harvesting method influences results of apoptosis analysis by annexin V staining. *Anticancer Res.* **2013**, *33* (8), 3201−3204.
(122) Galluzzi, L.; Aaronson, S.; Abrams, J.; Alnemri, E.; Andrews, D.; Baehrecke, E.; Bazan, N.; Blagosklonny, M.; Blomgren, K.; Borner, C.; et al. Guidelines for the use and interpretation of assays for monitoring cell death in higher eukaryotes. *Cell Death Differ.* **2009**, *16* (8), 1093.
(123) Yang, J.; Liu, X.; Bhalla, K.; Kim, C. N.; Ibrado, A. M.; Cai, J.; Peng, T.-I.; Jones, D. P.; Wang, X. Prevention of apoptosis by Bcl-2: release of cytochrome c from mitochondria blocked. *Science* **1997**, *275* (5303), 1129−1132.
(124) Chipuk, J. E.; Kuwana, T.; Bouchier-Hayes, L.; Droin, N. M.; Newmeyer, D. D.; Schuler, M.; Green, D. R. Direct activation of Bax by p53 mediates mitochondrial membrane permeabilization and apoptosis. *Science* **2004**, *303* (5660), 1010−1014.
(125) Zabirnyk, O.; Yezhelyev, M.; Seleverstov, O. Nanoparticles as a novel class of autophagy activators. *Autophagy* **2007**, *3* (3), 278−281.
(126) Seleverstov, O.; Zabirnyk, O.; Zscharnack, M.; Bulavina, L.; Nowicki, M.; Heinrich, J.-M.; Yezhelyev, M.; Emmrich, F.; O'Regan, R.; Bader, A. Quantum dots for human mesenchymal stem cells labeling. A size-dependent autophagy activation. *Nano Lett.* **2006**, *6* (12), 2826−2832.
(127) Chen, Z.; Bachhuka, A.; Han, S.; Wei, F.; Lu, S.; Visalakshan, R. M.; Vasilev, K.; Xiao, Y. Tuning chemistry and topography of nanoengineered surfaces to manipulate immune response for bone regeneration applications. *ACS Nano* **2017**, *11* (5), 4494−4506.
(128) Mao, A. J.; Bechberger, J.; Lidington, D.; Galipeau, J.; Laird, D. W.; Naus, C. C. Neuronal differentiation and growth control of neuro-2a cells after retroviral gene delivery of connexin43. *J. Biol. Chem.* **2000**, *275* (44), 34407−34414.
(129) Sato, C.; Matsuda, T.; Kitajima, K. Neuronal differentiation-dependent expression of the disialic acid epitope on CD166 and its involvement in neurite formation in Neuro2A cells. *J. Biol. Chem.* **2002**, *277*, 45299.
(130) Gusel'Nikova, V.; Korzhevskiy, D. NeuN as a neuronal nuclear antigen and neuron differentiation marker. *Acta Naturae* **2015**, *7* (2), 42.
(131) Sarnat, H. B.; Nochlin, D.; Born, D. E. Neuronal nuclear antigen (NeuN): a marker of neuronal maturation in the early human fetal nervous system1. *Brain Dev.* **1998**, *20* (2), 88−94.
(132) Herculano-Houzel, S.; Lent, R. Isotropic fractionator: a simple, rapid method for the quantification of total cell and neuron numbers in the brain. *J. Neurosci.* **2005**, *25* (10), 2518−2521.
(133) Sanchez-Ramos, J. R.; Song, S.; Kamath, S. G.; Zigova, T.; Willing, A.; Cardozo-Pelaez, F.; Stedeford, T.; Chopp, M.; Sanberg, P. R. Expression of neural markers in human umbilical cord blood. *Exp. Neurol.* **2001**, *171* (1), 109−115.

DOI: 10.1021/acs.nanolett.9b04216
Nano Lett. XXXX, XXX, XXX−XXX

(134) Cho, S.; Wood, A.; Bowlby, M. R. Brain slices as models for neurodegenerative disease and screening platforms to identify novel therapeutics. *Curr. Neuropharmacol.* **2007**, *5* (1), 19−33.
(135) Cho, S.; Liu, D.; Fairman, D.; Li, P.; Jenkins, L.; McGonigle, P.; Wood, A. Spatiotemporal evidence of apoptosis-mediated ischemic injury in organotypic hippocampal slice cultures. *Neurochem. Int.* **2004**, *45* (1), 117−127.
(136) Finley, M.; Fairman, D.; Liu, D.; Li, P.; Wood, A.; Cho, S. Functional validation of adult hippocampal organotypic cultures as an in vitro model of brain injury. *Brain Res.* **2004**, *1001* (1−2), 125−132.
(137) Laake, J. H.; Haug, F.-M.; Wieloch, T.; Ottersen, O. P. A simple in vitro model of ischemia based on hippocampal slice cultures and propidium iodide fluorescence. *Brain Res. Protoc.* **1999**, *4* (2), 173−184.
(138) Jones, K. H.; Senft, J. A. An improved method to determine cell viability by simultaneous staining with fluorescein diacetate-propidium iodide. *J. Histochem. Cytochem.* **1985**, *33* (1), 77−79.
(139) Mărgăritescu, O.; Mogoantă, L.; Pirici, I.; Pirici, D.; Cernea, D.; Mărgăritescu, C. Histopathological changes in acute ischemic stroke. *Romanian journal of morphology and embryology* **2009**, *50* (3), 327−339.
(140) Eng, L. F. Glial fibrillary acidic protein (GFAP): the major protein of glial intermediate filaments in differentiated astrocytes. *J. Neuroimmunol.* **1985**, *8*, 203−214.
(141) Liddelow, S. A.; Guttenplan, K. A.; Clarke, L. E.; Bennett, F. C.; Bohlen, C. J.; Schirmer, L.; Bennett, M. L.; Münch, A. E.; Chung, W.-S.; Peterson, T. C.; et al. Neurotoxic reactive astrocytes are induced by activated microglia. *Nature* **2017**, *541* (7638), 481.
(142) Imai, Y.; Ibata, I.; Ito, D.; Ohsawa, K.; Kohsaka, S. A novel geneiba1in the major histocompatibility complex class III region encoding an EF hand protein expressed in a monocytic lineage. *Biochem. Biophys. Res. Commun.* **1996**, *224* (3), 855−862.
(143) Papa, S.; Rossi, F.; Ferrari, R.; Mariani, A.; De Paola, M.; Caron, I.; Fiordaliso, F.; Bisighini, C.; Sammali, E.; Colombo, C.; et al. Selective nanovector mediated treatment of activated proinflammatory microglia/macrophages in spinal cord injury. *ACS Nano* **2013**, *7* (11), 9881−9895.
(144) Minami, S. S.; Sun, B.; Popat, K.; Kauppinen, T.; Pleiss, M.; Zhou, Y.; Ward, M. E.; Floreancig, P.; Mucke, L.; Desai, T.; et al. Selective targeting of microglia by quantum dots. *J. Neuroinflammation* **2012**, *9* (1), 22.
(145) Blasi, E.; Barluzzi, R.; Bocchini, V.; Mazzolla, R.; Bistoni, F. Immortalization of murine microglial cells by a v-raf/v-myc carrying retrovirus. *J. Neuroimmunol.* **1990**, *27* (2−3), 229−237.
(146) Stansley, B.; Post, J.; Hensley, K. A comparative review of cell culture systems for the study of microglial biology in Alzheimer's disease. *J. Neuroinflammation* **2012**, *9* (1), 115.
(147) Xiao, L.; Zhou, Y.; Zhu, L.; Yang, S.; Huang, R.; Shi, W.; Peng, B.; Xiao, Y. SPHK1-S1PR1-RANKL Axis Regulates the Interactions Between Macrophages and BMSCs in Inflammatory Bone Loss. *J. Bone Miner. Res.* **2018**, *33* (6), 1090−1104.
(148) Tremblay, R. G.; Sikorska, M.; Sandhu, J. K.; Lanthier, P.; Ribecco-Lutkiewicz, M.; Bani-Yaghoub, M. Differentiation of mouse Neuro 2A cells into dopamine neurons. *J. Neurosci. Methods* **2010**, *186* (1), 60−67.
(149) Minana, M.-D.; Felipo, V.; Grisolia, S. Inhibition of protein kinase C induces differentiation in Neuro-2a cells. *Proc. Natl. Acad. Sci. U. S. A.* **1990**, *87* (11), 4335−4339.
(150) Humpel, C. Organotypic brain slice cultures: A review. *Neuroscience* **2015**, *305*, 86−98.
(151) Tasca, C. I.; Dal-Cim, T.; Cimarosti, H. In vitro oxygen-glucose deprivation to study ischemic cell death. *Methods Mol. Biol.* **2015**, *1254*, 197−210.
(152) Wu, C.; Zhou, Y.; Fan, W.; Han, P.; Chang, J.; Yuen, J.; Zhang, M.; Xiao, Y. Hypoxia-mimicking mesoporous bioactive glass scaffolds with controllable cobalt ion release for bone tissue engineering. *Biomaterials* **2012**, *33* (7), 2076−2085.
(153) Bookout, A. L.; Mangelsdorf, D. J. Quantitative real-time PCR protocol for analysis of nuclear receptor signaling pathways. *Nucl. Recept. Signaling* **2003**, *1*, nrs.01012.
(154) Bustin, S. A.; Benes, V.; Garson, J. A.; Hellemans, J.; Huggett, J.; Kubista, M.; Mueller, R.; Nolan, T.; Pfaffl, M. W.; Shipley, G. L.; et al. The MIQE guidelines: minimum information for publication of quantitative real-time PCR experiments. *Clin. Chem.* **2009**, *55* (4), 611−622.

DOI: 10.1021/acs.nanolett.9b04216
Nano Lett. XXXX, XXX, XXX−XXX